General Disclaimer

One or more of the Following Statements may affect this Document

- This document has been reproduced from the best copy furnished by the organizational source. It is being released in the interest of making available as much information as possible.

- This document may contain data, which exceeds the sheet parameters. It was furnished in this condition by the organizational source and is the best copy available.

- This document may contain tone-on-tone or color graphs, charts and/or pictures, which have been reproduced in black and white.

- This document is paginated as submitted by the original source.

- Portions of this document are not fully legible due to the historical nature of some of the material. However, it is the best reproduction available from the original submission.

Produced by the NASA Center for Aerospace Information (CASI)

NASA

Technical Memorandum 85100

METHODOLOGY FOR
INTERPRETATION OF SST
RETRIEVALS USING THE
AVHRR SPLIT WINDOW
ALGORITHM

R.W. Barbieri, C.R. McClain and
D.L. Endres

SEPTEMBER 1983

METHODOLOGY FOR INTERPRETATION OF SST RETRIEVALS USING THE AVHRR SPLIT WINDOW ALGORITHM

Richard W. Barbieri   and   Charles R. McClain

Laboratory for Atmospheric Sciences

NASA/Goddard Space Flight Center

and

Daniel L. Endres

Instrument Systems Division

NASA/Goddard Space Flight Center

ABSTRACT

Intercomparisons of sea surface temperature (SST) products derived from the operational NOAA-7 AVHRR-II algorithm and in situ observations are made. The 1982 data sets consist of ship survey data during the winter from the Mid-Atlantic Bight (MAB), ship and buoy measurements during April and September in the Gulf of Mexico and shipboard observations during April off the N.W. Spanish coast. The analyses included single pixel comparisons and the warmest pixel technique for 2 X 2 pixel and 10 X 10 pixel areas. The reason for using multipixel areas was for avoiding cloud contaminated pixels in the vicinity of the field measurements. Care must be taken when applying the warmest pixel technique near oceanic fronts. The Gulf of Mexico results clearly indicate a persistent degradation in algorithm accuracy due to El Chichon aerosols. The MAB and Spanish data sets indicate that very accurate estimates can be achieved if care is taken to avoid clouds and oceanic fronts.

List of Tables

List of Figures

I. Introduction

In the early 1960's scientific attention was focussed on doing astrophysics from satellities, well above the interference of the earth's atmosphere. By the late 1960's there was an increasing interest in making observations of the earth from satellites. Sensors, formerly used for astrophysical observations in the infrared and microwave regions, were pointed towards earth. A succession of improvements were made in sensor technology and associated algorithms were developed to convert the raw data into physically meaningful parameters. By the late 1970's and early 1980's, a four wavelength infrared radiometer (VHRR, Very High Resolution Radiometer) was in wide use to study the oceans. The algorithms used to extract sea surface temperature (SST) from the data gathered by this instrument suffered from some deficiencies: clouds in the field of view, poor correction for the presence of atmospheric constituents, an inability to track low-latitude moisture variation etc. In late 1981 a five wavelength infrared radiometer (AVHRR-II, Advanced Very High Resolution Radiometer) became available; its primary advantage was to allow for a more accurate correction for the presence of water vapor in the atmosphere. One of the algorithms developed to extract SST has been used to carry out the analysis presented in this report.

As it is with the development of any new algorithm, a period of time must be invested to accumulate experience using the algorithm and to gain confidence in its applicability to a variety of problems. In particular, with a SST algorithm, confidence becomes established only after the performance of the algorithm in a variety of oceanographic and atmospheric conditions is documented. However what this entails is the arduous task of establishing a scientific methodology for interpretation of the SST retrievals produced by the algorithm.

This report represents our contributions to the establishment of a methodology. As will be shown, one major conclusion of our analysis is that the methodology must be adaptive; that is, interpretation of SST retrievals must be carried out with full awareness of atmospheric conditions and the presence of oceanographic gradients.

II. Data Processing
Satellite/Instrument

This study has utilized the AVHRR-II on the NOAA-7 satellite launched in June 1981. The nominal orbital characteristics are listed in Table 1 and the wavelength bands for each channel are presented in Table 2.

The instantaneous field of view (IFOV) of each channel is approximately 1.4 milliradians; at the nominal altitude this yields a sub-satellite point resolution of 1.1 km. Digitization of the analog data output from each channel occurs onboard the spacecraft at a rate of 39,936 samples per second per channel yielding 1.362 samples per IFOV. The AVHRR scans at a rate of 6 revolutions per second. Each scan of the earth spans an angle of ±56° about the sub-satellite track and produces a total of 2048 samples per channel. The data is digitized to 10 bit precision and this data is selectively recorded onboard the spacecraft for playback as Local Area Coverage (LAC) data. Only ten minutes of LAC data may be recorded per orbit. The data sets received from NOAA were LAC data sets with calibration coefficients and navigation information supplied on the tape. For more detailed information about this instrument see Lauritson(1979) and Kidwell(1981).

The NOAA data tapes containing the LAC information were processed at GSFC using an HP1000 computer system with an interactive image analysis capability. The software calibrates and maps this data utilizing the projection selected

from among various options. These data are mapped either as percent albedo (for channels 1 and 2), brightness temperature (for channels 3, 4 and 5) or SST (using the daytime split window algorithm). Percent albedo is the ratio (x100) of the measured radiance in channel two to the radiance that would be observed from a 100% reflecting, Lambertian surface when the solar zenith angle is zero. Once the data are mapped, one can interactively analyze the data in several ways. Software exists for plotting, making histograms, combining various channels so as to manually compute SST using the daytime/nightime algorithms, masking, shifting pictures to ensure proper navigation, or zooming in on areas of particular interest. Many other capabilities exist and are described along with those just mentioned in Goff(1983).

Sources of Error

The infrared radiation emitted from the surface of the ocean is altered by several environmental factors; consequently, the total radiance that finally impinges upon the sensor aperture is not the radiance emitted from the surface but rather a distortion of it. There are three sources of error in the infrared wavelength band 10.5 μm - 12.5 μm. One is solar reflection; this error source makes a very small contribution to channels 4 and 5 but has a significant effect on channel 3. Another source of error is the appearance of clouds in the field of view of the radiometer. As Maul (1981) mentions, if as little as 10% of the radiometers field of view is cloud contaminated an error of -0.5°C can be imparted to the SST retrieval; Bernstein (1982) also dicusses the effects of unresolved clouds. The last source of error and the one which leads to the largest magnitude of distortion of the original signal is the presence of an absorbing atmosphere. According to Maul and Sidran (1973), an rms error of ±0.3°K to ±0.6°K can be imparted to an SST retrieval by the presence of

3

atmospheric water vapor and other constituents. Another potentially large source of error, unrelated to radiometric considerations, results from navigation errors. The data tapes provided by NOAA contain navigation information for every 40th pixel along each scan line. This navigation, however, may be several kilometers in error. This is precisely what was found in the New England Shelf data set. The ship tracks in this winter data set started in the cold near-shore waters and terminated near the north wall of the Gulf Stream. The sharp gradients that were found along these ship tracks required that the satellite observations be carefully navigated to prevent large SST differences between the ship and the satellite measurements due solely to the fact that the measurements were made in different places. This data set was corrected by using four landmarks found in visible images on each day of the set.

Sea-Surface Temperature Retrieval Algorithm

The sea surface temperature retrieval algorithm used in this study has been developed by McClain and his colleagues at NOAA/NESS (McClain,1981). The algorithm represents the culmination of work carried on over the past dozen years: Anding and Kauth (1970), Prabhakara, Dalu and Kunde (1974), Deschamps and Phulpin (1980). The main idea underlying the split window algorithm used in this report stems from the variation of atmospheric transmittance in the 10.5 to 12.5 μm window. In particular, if this window is split into two bands it is found that the transmittance in the 11.5 μm - 12.5 μm window is less than the transmittance in the 10.5 μm - 11.5 μm window. This difference is interpreted as being due to the response of each channel to the total amount of water in the air column. The SST retrieval technique makes use of this difference in the two measurements to arrive at a correction for the atmospheric attenuation in the 10.5 μm - 11.5 μm window.

The sea surface temperature retrieval algorithms are given in Table 3.

4

It is noted that slightly different coefficients appear in the equations pertaining to daytime and nighttime passes.

Extraction of Water Vapor

J. Gatlin et al. (1982) presented an example of the water vapor excraction capability of the algorithm using Global Area Coverage (GAC) data which has a resolution of 4 kilometers. A particularly useful scene for this purpose was taken on October 3, 1981 over the Gulf of Mexico; see figures 1, 2 and 3. Figure 1, the channel 2 image, shows a small amount of cloud cover over the Gulf of Mexico north of Cuba and west of Florida. On the other hand, figures 2 and 3, representing channels 4 and 5 respectively, show a prominant moist tongue extending eastward across Florida with highly contrasting dry air to the north and south of the tongue. Also shown in these three figures are north-south transects made through the moist tongue. Figure 4 shows plots of channels 2, 4, and 5 along the transect. Channel 2 is presented as percent albedo while channels 4 and 5 are given in brightness temperature. Channel 2 shows a slight increase in percent albedo in passage from north to south along the transect. Clouds are clearly discernable as spikes first occuring about 400 km from the northern edge. Channels 4 and 5 brightness temperatures are nearly the same along the first 100km of the transect; what this means is that there is very little moisture in the atmosphere to perturb the signal in the 11.5 - 12.5 window. Since the presence of atmospheric water vapor is the major source of error, the agreement between the two channels is interpreted as being indicative of the presence of dry air. As the transect is followed further south the moist tongue is entered and this shows up in figure 4 as a divergence in the brightness temperatures of channels 4 and 5. The moist tongue ends around 480 km from the northern edge of the transect; this is evidenced by the convergence of channels 4 and 5. Continuing south, the water vapor content in the atmosphere

5

begins to increase as evidenced by the divergence of channels 4 and 5; finally at the tip of Cuba the brightness temperatures are not only widely separated but are also smaller in magnitude than at the northern edge of the transect. This is attributable, as will be discussed, to increased atmospheric water vapor rather than to a cooling of surface water at the southern edge of the transect. Figure 5 shows the results of the use of the split window algorithm. It is immediately clear that the SST has a monotonic increasing trend as expected along a north-south transect in the Gulf of Mexico during this time of year. The effects of clouds are also plainly evident especially at the southern end of the transect. In this example the algorithm was applied only where the albedo was less than six percent. This screened out the major clouds filling a large portion of the IFOV, but allowed some to remain as exemplified by the spike at 440km. It is noted that those clouds which remained in the field of view significantly lowered the estimated value of the SST.

Figure 6 shows the SST map which is derived from the application of the split window algorithm. It is of most interest to note the Loop Current hugging the Cuban coast; this feature would not be seen with the older instruments in which channel 4 spanned the entire 10.5 μm - 12.5 μm range. The moist tongue, evident in channels 4 and 5 (Figures 2 and 3), has clearly been removed by this algorithm.

III. Data Sets

The data sets which have been analyzed for this report are comprised of ship board measurements, buoy measurements and satellite measurements. The time periods covered by this data are summarized below:

Southern New England Shelf: Dec. 14, 1981 - March 29, 1982

West Florida Shelf: March 31, 1982 - April 7, 1982

West Spanish Coast: April 10, 1982 - April 29, 1982

West Florida Shelf: Sept. 9, 1982 - Sept. 22, 1982

The useable AVHRR data is a subset of the data listed above because of the frequent appearance of clouds. In particular useable AVHRR data have been identified for the following dates:

Southern New England Shelf: Jan 27, Feb 8, March 29

West Florida Shelf: March 31, April 1,2,3,4,7

West Spanish Coast: April 12,13,18,19,20,25,27,29

West Florida Shelf: Sept 10,13,16,17,18

IV.

Southern New England Shelf

During the period from October 1981 to March 1982, the Woods Hole Oceanographic Institution (WHOI) conducted a series of cruises primarily along 71°W longitude and ranging from 41°N to 39°N latitude. Out of 14 cruise dates only three occurred during periods of time when the cruise area was cloud free. The AVHRR derived SST's were compared with the in-situ data in three ways. The first method is to compare point for point, choosing that AVHRR SST which is closest to the location of the ship SST. The second and third ways pertain to constructing areas of different sizes centered on the ship location and choosing the warmest temperature within the area. The motivation for this procedure is two-fold: (1) the satellite data usually has navigation error embedded in it and, (2) in the presence of very thin or small clouds the warmest temperature most likely represents the sea surface. Two different sized areas were chosen: a two kilometer-by-two kilometer area and a ten kilometer-by-ten kilometer area each centered at the ship location. The comparisons for this data set are shown in Tables 4 through 6. Figure 7 shows the scatter plot of the WHOI/AVHRR single point comparison for all three days; this set is made up of 34 points. The average $\Delta T = -0.79°C$ with a standard deviation of $1.07°C$. The 95% confidence interval is $-1.15°C < \Delta T < -0.43°C$; $\Delta T = T_{AVHRR} - T_{SHIP}$.

Figure 8 shows the scatter plot of the WHOI/AVHRR two kilometer-by-two kilometer area comparison for all three days; this set is made up of 35 points. The average $\Delta T = -0.28°C$ with a standard deviation of 0.96°C. The 95% confidence interval is $-0.59°C < \Delta T < +0.00°C$.

Figure 9 shows the scatter plot of the WHOI/AVHRR ten kilometer-by-ten kilometer area comparison for all three days; it is comprised of 35 points. The average $\Delta T = + 0.62°C$ with a standard deviation of 1.30°C. The 95% confidence interval is $+0.19°C < \Delta T < +1.05°C$. This is the only scatter plot in which the bias is positive; the AVHRR SST tends on the average to be warmer than the ship temperature because of the influence of the area averaging close to the much warmer Gulf Stream waters.

Figure 10 shows the AVHRR SST plot along the ship cruise track on Jan. 27, 1982. The top curve is the SST plot and the bottom curve is a plot of channel 2 along the same track. The corresponding ship SST's are shown as circles. The agreement between the two types of data is very good out to around line 100 where the albedo begins to exceed 5%. As noted by Maul and Sidran (1973) and Bernstein (1982) the effects of unresolved clouds can be appreciable. This New England Shelf data set is particularly useful for providing a statistical measure of these effects because the atmosphere tends to be dry and hence the water vapor absorption problem tends to be minimized. An indication of these effects was derived as follows. Each 2km x 2km or 10km x 10km area, centered at the ship location, was evaluated for total cloud content in the area. A value of 0 was assigned to the area if there were no clouds; a value of 1 was assigned if less than a third of the area had clouds and, a value of 2 was assigned if two thirds or more of the area had clouds. A 6% albedo was used to flag cloudy pixels. The results are summarized in Table 7 and Table 8 for those areas where a value of zero or one was assigned.

8

Note that the total of 35 points of the original data set has been reduced by no less than 25%. In the column marked single point, the ΔT is slightly lower than when all the points are used (Fig.7); however the standard deviation is reduced by more than 50%. In the 2 km x 2 km column the ΔT increases by at least 30% in each case over the ΔT found when all the points were used (Fig. 8); once again though the standard deviation of ΔT is reduced by at least 50%. In the 10km x 10km area, the ΔT shows its greatest reduction from the value of + 0.62°C computed using all the points. A 50% reduction is also found in the standard deviation (Fig.9). The conclusion is that the effects of clouds can make a significant contribution to the confidence one has in the computed estimate of ΔT. The 3 σ values for the case when the cloud index = 0 never exceeds 1.35°C; the 10km x 10km area yields the largest standard deviation because of the influence of the warmer Gulf Stream water within the averaging area.

V.

West Florida Shelf

During the period April 2, 1982 through April 7, 1982 and from Sept. 13, 1982 through Sept. 18, 1982, the Skidaway Institute of Oceanography conducted a survey along the west Florida shelf within the area shown in Figure 11. High quality ship and bucket SST's were collected and accurately tagged with latitude and longitude information. In addition to these data, some environmental buoy and ship-of-opportunity data which coincided with the two Skidaway cruise periods were also collected. The purpose of the cruises was to observe Loop Current interactions with the waters of the west Florida continental shelf. These exchange processes should be similar to those on the east Florida shelf since the Loop Current and Florida Current are parts of the Gulf Stream system

and possess the same frontal wave features. During the spring 1982 cruise, a large filament (frontal wave) propagated through the experiment site and was tracked using the satellite imagery. Figure 12 shows the movements of the filament on five consecutive days and the eastward translation of the Loop Current front downstream of the filament. The phase velocity of the wave was approximately 30 cm/sec. A filament is a 'folded-back' wave whose circulation is described in McClain et al., (1983). A detailed description of this particular event is discussed in Paluszkiewicz et al. (1983).

As with the WHOI data set, the SST's derived from AVHRR were compared with the ship and buoy data in the same three ways as discussed in section IV. The comparisons of the springtime data is shown in Table 9. The comparison of the September data is shown in Table 10.

Figure 13 shows the scatter plot of the single point comparison over the springtime data set which is made up of 30 points. The average $\Delta T = -2.03°C$ with a standard deviation of 1.01°C. The 95% confidence interval is -2.40°C < ΔT < -1.65°C.

Figure 14 shows the scatter plot of the 2km x 2km area comparison over the springtime data set. This set is also comprised of 30 points with an average $\Delta T = -1.59°C$ and a standard deviation of 0.84°C. The 95% confidence interval is given by -1.90 < ΔT < -1.27°C.

Figure 15 shows the scatter plot of the 10km x 10km area comparison over the spring time data set. This set is made up of 31 points with an average $\Delta T = -1.20°C$ and a standard deviation of 0.74°C. The 95% confidence interval is -1.46°C < ΔT < -0.94°C.

Figures 16, 17 and 18 pertain to the September data set. The single point comparison scatter plot, shown in figure 16, yields an average T = -2.29°C and standard deviation of 1.21°C. The 95% confidence interval is given by

10

-2.99°C < ΔT < 1.59°C. There are 14 points in this set.

The 2km x 2km area comparison scatter plot is shown in figure 17. The average ΔT = - 1.68°C with a standard deviation of 0.61°C. The 95% confidence interval, for 14 points, is given by -2.03°C < ΔT <-1.32°C.

Figure 18 shows the ten-by-ten area comparison scatter plot made up of 16 points. The average ΔT = - 1.17°C with a standard derivation of 0.73°C. The 95% confidence interval is given by -1.55°C < ΔT <- 0.78°C.

The effects of clouds in the field of view was evaluated in the same way as was done in Section IV. Here, only ship data from the springtime data set was used. The results are summarized in Tables 11 and 12. The curious thing about this data set is that when cloud free images are considered the ΔT increases very slightly when compared against slightly cloudy conditions(cloud index = 1). This may simply be a numerical accuracy problem. The real point is that the two comparisons show no significant change. Our conjecture is that the large values of ΔT and σ are caused by the large spatial and temporal variability of surface phenomena and the effects of the El Chicon volcano which erupted at the end of March. The surface variability is brought out by looking at the April ship cruise data; it yields a standard deviation of about 1.2°C. An assessment of the effects of El Chicon on AVHRR/SST data has been made by Strong et al (1982).

VI.

West Spanish Coast

April 18-22 1982

During the past ten years, an intensive study of upwelling within the rias of NW Spain has been underway. The waters of the rias support one of the most productive aquacultures (mussels) in the worl(The nutrient source for this system is coastal upwelling on the continental s, ,. Tidal circulation then moves

11

these waters into the rias (Tenore, et al, 1982). The specific mechanisms which produce this upwelling have not been studied in detail since previous work has been confined to the rias themselves. The most likely cause is a general wind-driven upwelling such as that found off the Oregon coast with localized enhancement due to bathymetric effects, but these effects have not as yet been quantified. The April, 1982 cruises were the first attempt to investigate the shelf break upwelling.

During the period from April 18, 1982 through April 22, 1982 the Spanish American Rias Study (SARS) Group conducted a survey along the Galician coast of Spain. Figure 19 shows the SST data gathered during the survey.

Table 13 shows a comparison of several of the ship cruise SST's and the SST retrievals using the split window algorithm. The ship data has been chosen to correspond to ± 2 hours of the time of the satellite overpass. Because of this time constraint this data set is too sparse to make detailed AVHRR SST transects through the ship points. The comparisons of seven points shown in Table 13 shows agreement to within $1.2°C$. The 10x10km analysis yields a $\Delta T=-0.14°C$. The most interesting aspect of this data is a rather intriguing feature along the west coast of Spain which appeared in an IR image on April 29, 1982. The feature is clearly seen in figure 20. One constant longitude AVHRR transect was made across the feature and is shown in figure 21. Channels 1,2, 4 and 5 are plotted in addition to the SST derived from channels 4 and 5. The transect starts at a point north of the feature in a cloudy region as evidenced by the sharp, large magnitude spikes in channels 1 and 2. By the time line 19 is reached the cloud covered area is left behind and it is seen that channels 4 and 5 are pretty much coincident indicating a dry atmosphere. Proceeding south along the transect, the atmosphere remains dry until the latitude around line 37 is reached. In this region channels 4 and 5 not only sharply decrease but also diverge from each other indicating a rapid increase in the water

12

vapor content. However, channels 1 and 2 remain fairly quiescent not only near line 37 but throughtout the transect. It is concluded from this that the change in channels 4 and 5 near line 37 is not caused by the presence of high clouds. Channels 4 and 5 remain separated along the transect from line 37 to around line 75. The maximum difference between the two channels amounts to about 1.7°C.

Moving south of line 75 shows a return to a very dry atmosphere where $T_4 - T_5 \sim 0$. It is also seen that the southern part of the transect has an SST which is about 0.5°C warmer than the northern part. The cause of the feature has been narrowed to two possibilities: an upwelling and/or advection fog. The argument in favor of the feature being an upwelling is very strong as figures 22 thru 24 show; (these figures have been shared with us after private communications with J. O. Blanton and L. P. Atkinson of Skidaway Institute of Oceanography). The time series of temperatures at station 3 (42°26.6'N, 9°1.1'W) are shown in figure 22. An upwelling on April 19-20 is clearly shown; another upwelling around April 28-29 is also strongly suggested. The wind stress time series is shown in figure 23. Note the long duration of upwelling favorable winds dating from about April 10. For three days prior to the April 19-20 upwelling shown in figure 22, the wind stress has a steady component directed south. The upwelling, shown in figure 22 beginning on April 28, is most likely induced by the strong southerly wind stress components shown to occur on April 24-26.

A measure of the strength of an upwelling has been proposed by Bakum (1973) and is contained in an index derived from surface winds and the computed Ekman transport. A time series of the upwelling index through the month of April is shown in figure 24. The upwelling index is a measure of the volume transport per kilometer (Sverdrups/km) and it is noticed that on April 25 thru April 26

some of the largest transports occurred. Additional upwelling favorable events occurred on the 27th, 28th and 29th of April although these were about half the magnitude of the index on the 25th and 26th. The cold feature seen in the IR image on April 29th is a manifestation of the strong upwelling which occurred 3 three days previously and somewhat slowed down from decaying by the events of April 27th through April 29th. It is unfortunate LAC coverage on April 27th was not available. The GAC data does indicate that the feature was present on the 27th but was not as well developed. However, it is not evident as to why the channel 4 and 5 brightness temperatures separate over the feature.

The other explanation for the cause of the cold feature is that what is being viewed from space is advection fog. The wind direction, as shown in figure 23, is not out of the north but has a northeasterly component. Wind from the northeast presumably has a temperature which is warmer than the underlying sea surface and will surrender heat to the ocean. Since the conductive capacity of water is much larger than that of air, the air must adjust it's temperature to the temperature of the water thereby increasing the relative humidity; condensation can begin and fog can develop. Note that this process occurs only with an ocean surface temperature cooler than the air temperature so that the upwelling mechanism and the advection fog mechanism are not mutually exclusive. Without the luxury of having in-situ data, the question is difficult to resolve. However, the real point of this discussion is that without a split-window instrument, the argument becomes vacuous. Only with an instrument which splits the 10.5 μm - 12.5 μm in half can the change in water vapor content be inferred.

Conclusions

In this report we have focussed on the comparison of in-situ and AVHRR-II SST. The data sets were obtained from the New England region south of Cape Cod

during the winter of 1981-1982, the West Florida Shelf during April and September 1982 and the Spanish coast during April 1982. Some comments on dynamical features observed in the imagery have been given, but detailed discussions will appear in other publications. The analysis employed the warmest pixel technique whereby the SST used was the warmest value within 3 different sized areas (single point, 2x2 pixels and 10x10 pixels). Additional analysis included cloud screening where the number of cloud contaminated pixels within the area was used as the criteria for eliminating a data point. A pixel was considered cloud covered if the percentage of albedo as measured by channel 2 exceeded 6%. The SST algorithm used was the NOAA operational analysis prior to the El Chicon eruption. No attempt to modify the algorithm to correct for upper atmosphere aerosols was made.

The analysis of the New England data shows that care must be taken when selecting the area used in the warmest pixel technique because oceanic fronts like the Gulf Stream can introduce artificially high values. In this case the 10kmx10km analysis with the most stringent cloud screening criteria (zero clouds) produced the lowest ΔT, +0.13°C. Since clouds generally form over the Gulf Stream front in the winter, the cloud screening also eliminated data near high SST gradients. Also, the water vapor content is a minimum during the winter and the dust cloud from El Chicon was not present.

The Gulf of Mexico data sets, while being separated in time by five months, produced very consistent results. El Chicon erupted three days before the first data set was collected. In both data sets the 10kmx10km area yielded the lowest ΔT, 1.2°C, which is an order of magnitude larger than that of the New England data set. Also, unlike the New England data, cloud screening did not improve the result even though the Loop Current front was within the survey area. The reason may be that clouds do not form along this front and, consequently, the SST gradient across this front is substantially smaller than that across the New

15

England sector of the Gulf Stream in the winter. It is difficult to determine if the larger bias in temperature found in the Gulf of Mexico was a result of the El Chicon aerosols or poor water vapor correction. The -1.2°C bias observed in April is in good agreement with the 1.0°C-1.5°C negative bias found by Strong et al. (1982) for the month of May. They report that by April 4 the bias had reached -1.5°C, also in close agreement with our values. Prior to the eruption, they report biases less than 0.5°C. Their analysis for September indicates biases ranging from 0.5°C-1.0°C, somewhat lower than our lowest value of -1.2°C.

Most of the data presented in this report had scan angles less than 40°. A check was made on the scan angle dependence of the derived SST. Our preliminary finding is that the SST retrieval is adversely affected but not enough data points are available to do a statistical analysis.

REFERENCES

Anding, D. and Kauth, R., (1970) " Estimation of Sea Surface Temperature
from Space", Remote Sensing of the Environment, vol. 1, pp 217-220.

Bakun, A., 1973 "Coastal Upwelling Indices, West Coast of North America, 1946-1971."
U.S. Department of Commerce, NOAA TECH. Rept. NMFS SSRF-671.

Bernstein, R. L., (1982), "Sea Surface Temperature Estimation Using the NOAA
6 Satellite Advanced Very High Resolution Radiometer", J. Geophys. Res.,
vol. 87, No. C12, pp 9455-9465.

Deschamps, P.Y. and Phulpin, T., (1980) "Atmospheric Correction of Infrared
Measurements of Sea Surface Temperature Using Channels at 3.7, 11 and
12 μ m", Boundary-Layer Meteorology, vol.18, pp 131-143.

Gatlin, J. A., Endres, D. L. and McClain, E. P.(1982), "Detection and Removal
of Water Vapor Patterns from SST Image Products Using the Split
Window Technique", AGU Spring Meeting, Philadelphia,PA.

Goff, T., (1983), " RAMTEK Image System Programs (A User's Guide), Unpublished
Report available from NASA/GSFC Code 972.

Kidwell, K.B., (1981), "NOAA Polar Orbiter Data User's Guide", NOAA/NESS.

Lauritson, L., (1979), "Data Extraction and Calibration of TIROS-N/NOAA
Radiometers", NOAA TM, NESS 107.

Maul, G.A. and Sidran, M., (1973), "Atmospheric Effects on Ocean Surface
Temperature Sensing from the NOAA Satellite Scanning Radiometer",
J. Geophys. Res., vol 78, No. 12, pp 1909-1916.

Maul. G.A., (1981), "Application of GOES Visible-Infrared Data to Quantifying
Mesoscale Ocean Surface Temperatures", J. Geophys. Res., vol. 86, No.
C9,pp 8007-8021.

McClain, E. Paul, (1981), "Multiple Atmospheric Window Techniques for Satellite
Derived Sea Surface Temperatures"; Oceanography from Space, edited by
J.F.R.Gower, Plenum Press.

McClain, C.R., Pietrefesa, L.J. and Yoder,J.A., (1983), "Observations of Gulf
Stream Induced and Wind Driven Upwelling in the Georgia Bight using
Ocean Color and Infrared Imagery", submitted to J. Geophys. Res.

Paluszkiewicz, T. Atkinson, L.P., Posmentier, E.S. and McClain, C.R., (1983),
"Observations of an Intrusion of a Loop Current Frontal Eddy onto
the West Florida Shelf", J. Geophys. Res. (in press).

Prabhakara, C., Dalu,G. and Kunde, V.G., (1974)," Estimation of Sea Surface
    Temperature from Remote Sensing inm the 11 μm to 13 μm Window Region",
    Boundary-Layer Meteorology, vol. 18, pp 131-143.

Strong, A., Gruber, A. and Stowe, L. (1982) "Effects of El Chicon Eruption
    on Satellite Observations", in NASA Technical Memoorandum 84959,
    edited by W. R. Bandeen and R. S. Fraser.

Tenore, K.R., Boyer,L.F., Cal, R.M., Corral, J., Garcia-Fernandez,C.,
Gonzalez, N., Gonzalez-Gurriaran,E., Hansen, R.B., Iglesias, J., Krom, M.,
Lopaz-Jamar, E., McClain, J., Pamaymat, M.M., Perez, A., Rhoads, D. C.,
deSantiago, G., Tietjen, J., Westrich, J. and Wimdon, H.L., (1982), " Coastal
    Upwelling in the Rias Balas, N.W. Spain: Contrasting the Benthic Regimes
    of the Rias de Arosa and deMuros", J. Marine Res., vol. 40, 3, pp 701-772.

TABLE 1

NOAA-7 ORBITAL CHARACTERISTICS

Altitude = 850km

Inclination = 99°

Ascending Node = 1430 local time

Descending Node = 0230 local time

Period = 102 minutes

Orbits/Day = 14.2

Repeat Cycle = 9.2 days

TABLE 2

NOAA-7 AVHRR Channels

CHANNEL	WAVELENGTH (μm)
1	0.55 - 0.68
2	0.725 - 1.1
3	3.55 - 3.93
4	10.3 - 11.3
5	11.5 - 12.5

TABLE 3

SEA SURFACE TEMPERATURE ALGORITHM

Daytime:
$$T_{sst} = 1.0351 \, T_4 + 3.0461(T_4 - T_5) - 10.78°K$$

Nighttime:
$$T_{sst} = 1.0527 \, T_4 + 2.6272(T_4 - T_5) - 15.07°K$$

where T_{sst} is sea surface temperature in °K

               T_4 is brightness temperature in °K from channel 4

               T_5 is brightness temperature in °K from channel 5

TABLE 4

Comparison with WHOI Ship Cruise Data

Jan 27, 1982

LAT(°N)	LONG(°W)	SHIP SST	AVHRR POINT	AVHRR 2x2	AVHRR 10x10
41.17	71.41	2.8	2.8	2.3	3.5
40.98	71.41	3.2	2.4	3.2	4.6
40.83	71.42	5.0	3.7	4.5	5.1
40.66	71.42	5.2	4.3	4.7	5.2
40.50	71.42	5.2	5.1	5.1	5.1
40.33	71.42	5.2	--	4.7	5.6
40.25	71.42	5.0	4.7	6.1	6.7
40.18	71.42	5.0	5.0	5.0	6.8
40.08	71.42	5.0	5.9	6.4	7.5
40.00	71.42	5.3	7.6	7.9	8.4
39.91	71.42	6.6	7.4	8.7	10.4
39.83	71.42	13.0	9.5	12.0	17.6

TABLE 5

Comparison with WHOI Ship Cruise Data

Feb 8, 1982

LAT(°N)	LONG(°W)	SHIP SST	AVHRR Point	AVHRR 2x2	AVHRR 10x10
41.17	70.86	2.7	1.8	1.9	2.4
40.90	70.74	3.5	3.0	3.5	3.6
40.83	70.56	4.5	3.4	4.2	4.2
40.67	70.50	3.3	2.3	2.4	3.3
40.50	70.38	3.0	2.3	2.3	3.0
40.33	70.25	1.8	1.9	1.9	2.3
40.26	70.19	3.2	1.7	1.7	2.5
40.17	70.13	5.0	1.8	2.2	4.4
40.08	70.12	5.2	2.7	4.6	5.8
40.00	69.99	5.3	4.6	4.8	6.0
39.91	69.93	5.6	4.7	5.9	8.1
39.83	69.87	(7	6.9	7.5	9.3
39.74	69.81	9.3	7.8	8.6	9.4
39.66	69.75	9.8	8.2	9.1	9.5

TABLE 6

Comparison with WHOI Ship Cruise Data

March 29, 1982

LAT(°N)	LONG(°W)	SHIP SST	AVHRR POINT	AVHRR 2x2	AVHRR 10x10
41.16	71.41	4.0	2.6	3.0	3.4
40.99	71.39	4.3	3.3	3.2	3.8
40.83	71.39	4.3	3.9	4.1	4.3
40.66	71.40	4.2	3.9	3.9	4.5
40.50	71.40	4.2	3.4	3.8	4.4
40.33	71.41	4.8	4.2	4.3	4.8
40.25	71.41	4.9	4.4	4.8	5.0
40.16	71.41	5.0	4.8	4.9	5.0
40.08	71.43	5.1	4.6	5.0	5.5

Table 7

Results for those areas for which cloud index = 1. (27 pts.)

	Single Point	2km x 2km	10km x 10km
ΔT	-0.75°C	-0.36°C	+0.34°C
σ	0.49°C	0.48°C	0.74°C

Table 8

Results for those areas for which cloud index = 0 (21 pts.)

	Single Point	2km x 2km	10km x 10km
ΔT	-0.67°C	-0.40°C	+0.13°C
σ	0.38°C	0.34°C	0.45°C

TABLE 9

WEST FLORIDA SHELF

COMPARISON OF AVHRR WITH SHIP AND BUOY DATA

MARCH 31, 1982 - APRIL 7, 1982

DATE	LAT(°N)	LONG(°W)	SHIP SST	BUCKET SST	BUOY SST	AVHRR POINT	AVHRR 2X2	AVHRR 10x10
3/31	26.0	86.0			26.6	23.25	24.5	24.97
	24.7	82.4	25.5			23.15	23.8	24.4
	25.9	89.7			23.3	22.45	22.8	22.85
	25.8	85.4	26.0			23.9	24.45	24.93
4/1	26.0	86.0			26.6	24.25	24.65	24.97
	24.7	82.4	25.6			24.4	24.4	25.12
	25.9	89.7			23.3	22.3	22.65	23.1
4/2	26.0	86.0			26.7	23.5	24.0	24.34
	25.4	85.6	26.7			24.1	24.5	24.88
	26.9	87.7	29.0			22.1	22.6	22.73
	25.66	84.3	26.1	25.9		24.8	24.8	25.07
	25.67	84.38	26.3	26.3		24.85	24.85	25.1
	25.55	84.47	26.3	26.2		22.95	24.95	25.1
	25.56	84.55	26.3	26.3		24.0	24.6	25.6
	25.9	89.7			23.6	21.85	22.2	22.58
4/3	26.0	86.0			26.9	24.3	24.75	25.17
	23.1	86.0	26.6			25.25	25.25	25.76
	24.6	86.6	25.8			21.95	24.3	24.54
	25.7	83.1	23.97	24.0		22.97	23.26	23.31
	25.68	83.41	24.2	24.4		23.31	23.31	23.41
	25.67	83.31	24.45	24.7		22.97	23.26	23.41
	25.66	83.20	24.1			23.07	23.07	23.41
4/4	26.0	86.0			26.7	21.75	22.0	23.1
	25.3	85.2	26.1					25.27
	26.16	84.69	25.3	25.3		22.61	22.95	23.41
	26.15	84.63	25.4	25.6		22.71	23.1	23.46
	26.16	84.55	25.6	26.0		23.49	23.54	23.51
	26.15	84.47	25.6	26.2		23.88	23.88	23.9
	26.15	84.34	25.2	25.5		23.49	23.54	23.9
	26.16	84.25	24.6	24.9		22.76	23.49	23.51
	26.17	84.15	23.8	24.0		22.27	22.6	23.22
4/7	27.25	83.78	22.6			22.14	22.52	22.92

TABLE 10

WEST FLORIDA SHELF

COMPARISON OF AVHRR WITH SHIP AND BUOY DATA

SEPT 10,1982 - SEPT 18, 1982

DATE	LAT(°N)	LONG(°W)	SHIP SST	BUCKET SST	BUOY SST	AVHRR POINT	AVHRR 2x2	AVHRR 10x10
9/10	26.0	86.0			28.9	27.3	27.3	28.59
9/13	25.9	89.7			28.7	27.85	28.25	28.25
	26.0	86.0			29.4	27.3	27.3	27.3
	26.9	86.9	27.8			26.45	26.45	27.8
	25.2	85.8	27.8			25.7	26.2	27.8
9/16	26.0	86.0			29.4	27.7		
9/17	26.0	86.0			29.6	27.7	28.05	28.10
	25.8	83.25	29.3			23.9	27.1	27.8
	25.79	83.33	29.1			25.95	27.95	28.34
	25.85	83.17	29.6			27.4	27.8	28.0
	25.77	83.44	29.3			25.45	27.1	27.7
9/18	25.7	83.6	29.6			28.7	28.7	29.0
	25.75	83.5	29.9			28.25	28.3	28.78
	25.77	83.44	29.9					28.44
	25.78	83.34	30.0			27.25	27.25	28.3
	25.81	83.25	29.6			27.3	27.3	27.3
	25.83	83.17	29.7					27.95

Table 11

Results for those areas for which cloud index = 1 (19 pts.)

	Single Point	2km x 2km	10km x 10km
ΔT	-1.66°C	-1.42°C	-1.10°C
σ	0.64°C	0.57°C	0.60°C

Table 12

Results for those areas for which cloud index = 0 (15pts.)

	Single Point	2km x 2km	10km x 10km
ΔT	-1.70°C	-1.44°C	-1.14°C
σ	0.69°C	0.64°C	0.66°C

TABLE 13

WEST SPANISH COAST

COMPARISON OF AVHRR AND SHIP DATA

APRIL 18,19,20, 1982

DATE	LAT(°N)	LONG(°W)	GMT	SHIP SST	AVHRR POINT	AVHRR 2x2	AVHRR 10x10
4/18	42.99	9.29	21.1	13.3	12.3	13.1	13.5
	42.99	9.34	21.3	13.3	12.9	13.1	13.5
	42.99	9.39	21.6	13.7	13.2	13.5	14.2
	43.0	9.44	21.8	13.7	13.1	13.1	13.5
4/19	42.44	9.02	18.6	13.3	13.0	13.4	13.5
4/20	42.55	9.21	16.3	14.27	13.2	13.2	13.6
	42.56	9.16	17.1	14.7	13.5	13.5	13.5
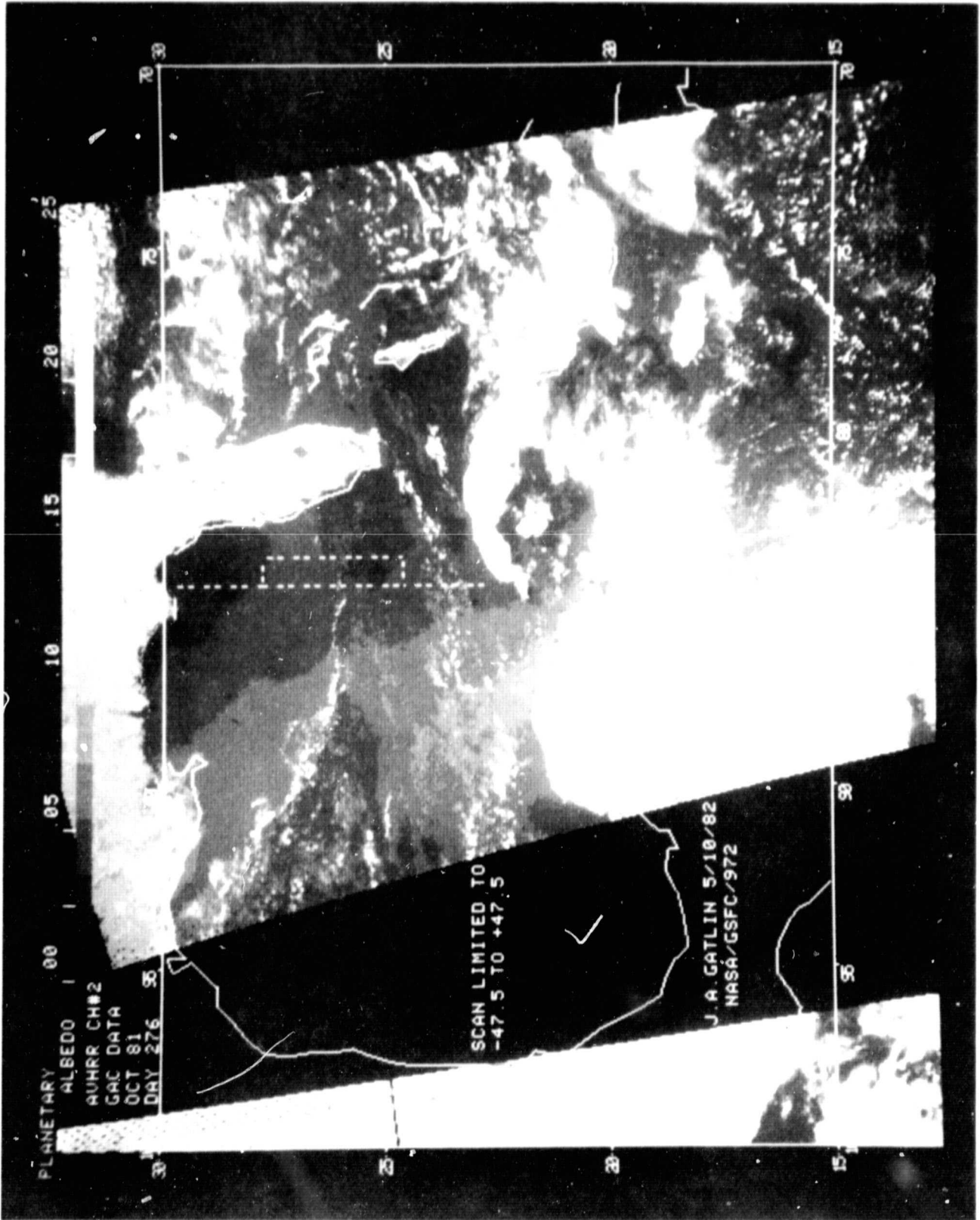
AVHRR CHANNEL 2 IMAGE
FIGURE 1

AVHRR CHANNEL 4 IMAGE
FIGURE 2
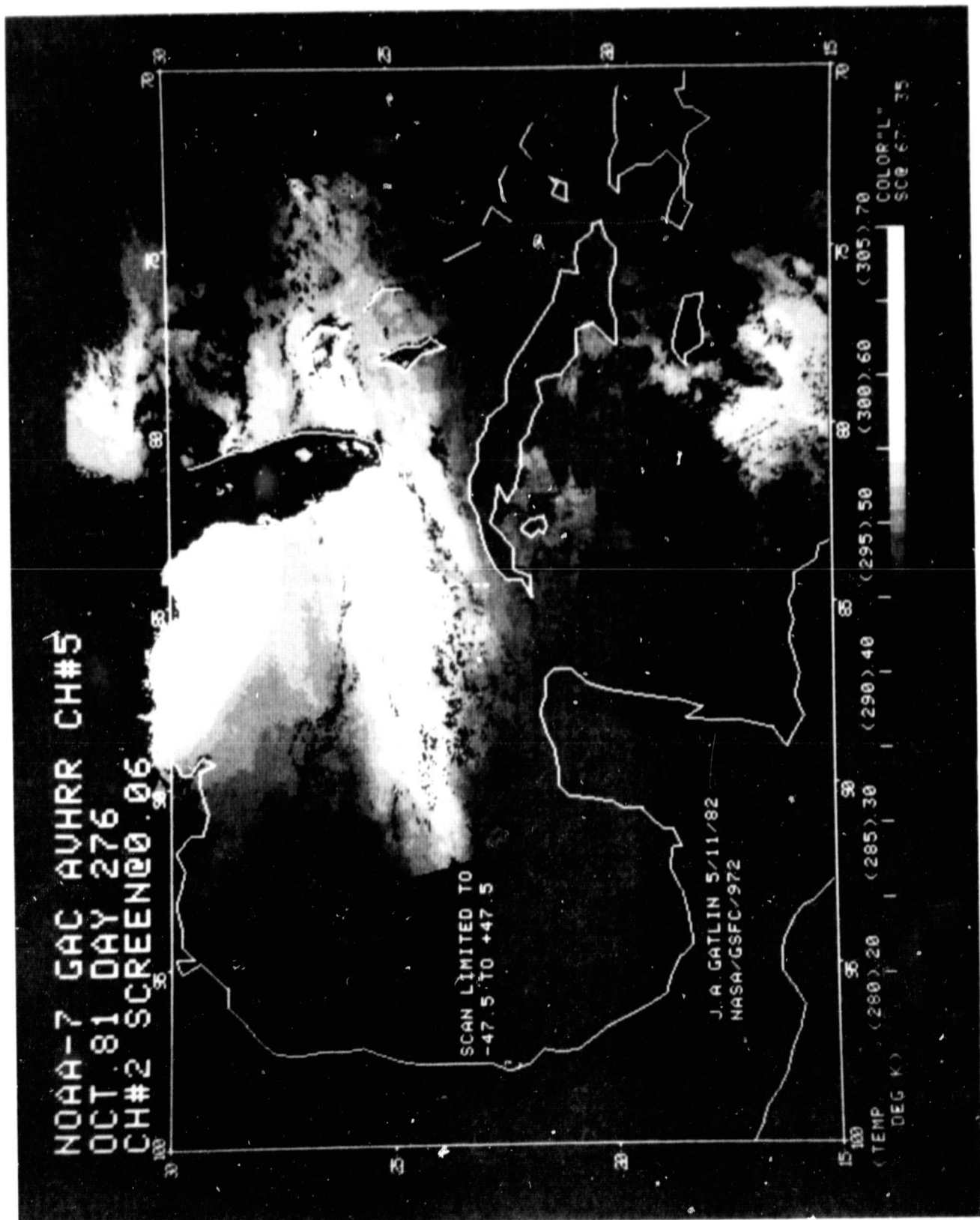
AVHRR CHANNEL 5 IMAGE
FIGURE 3
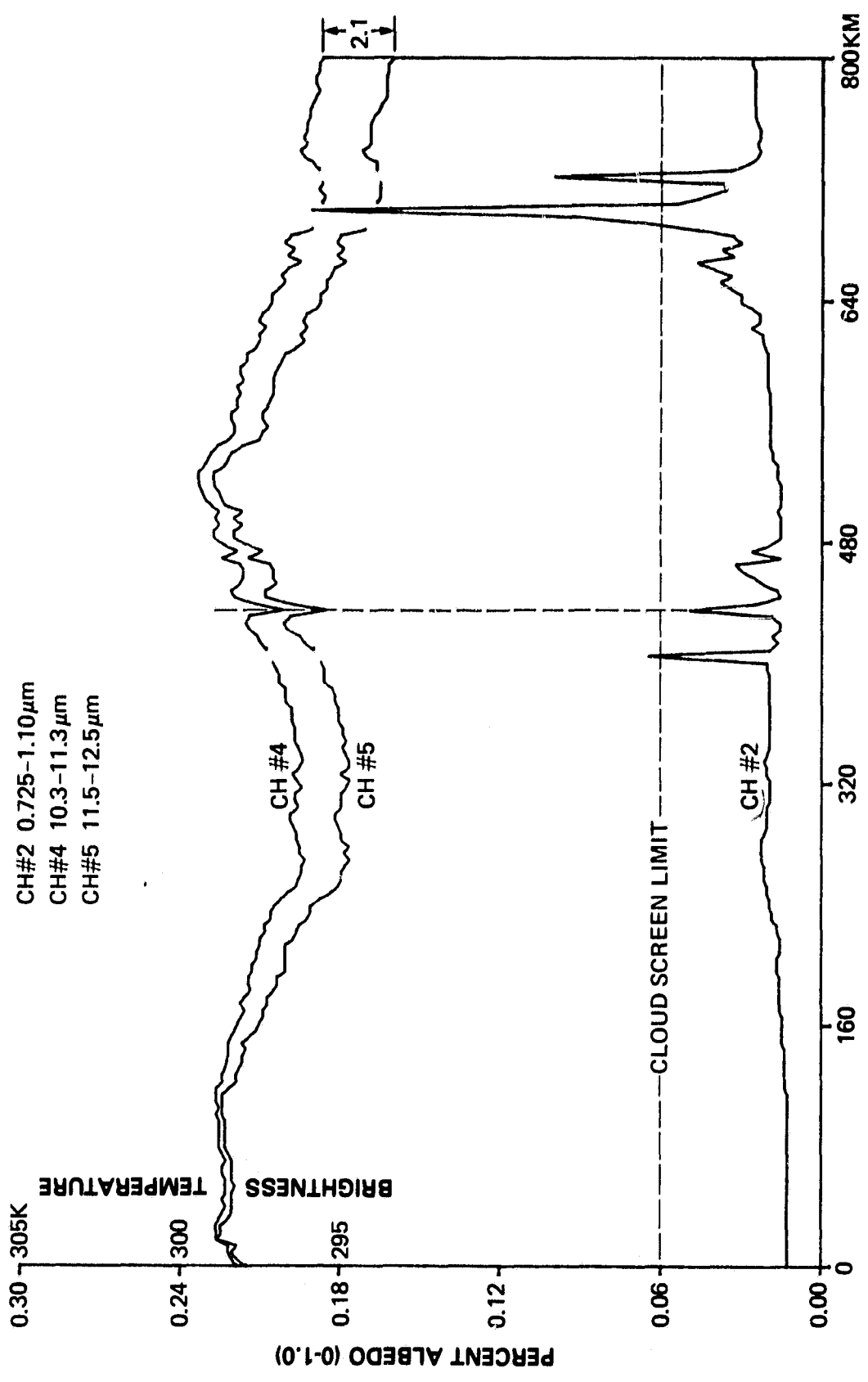
North-South Transects from NOAA-7 AVHRR, October 1981, Day 276

FIGURE 4

SST = CH #4 + 3.046 (CH #4 – CH #5) + BIAS
BIAS = (0.0351) CH #4 – 10.78K
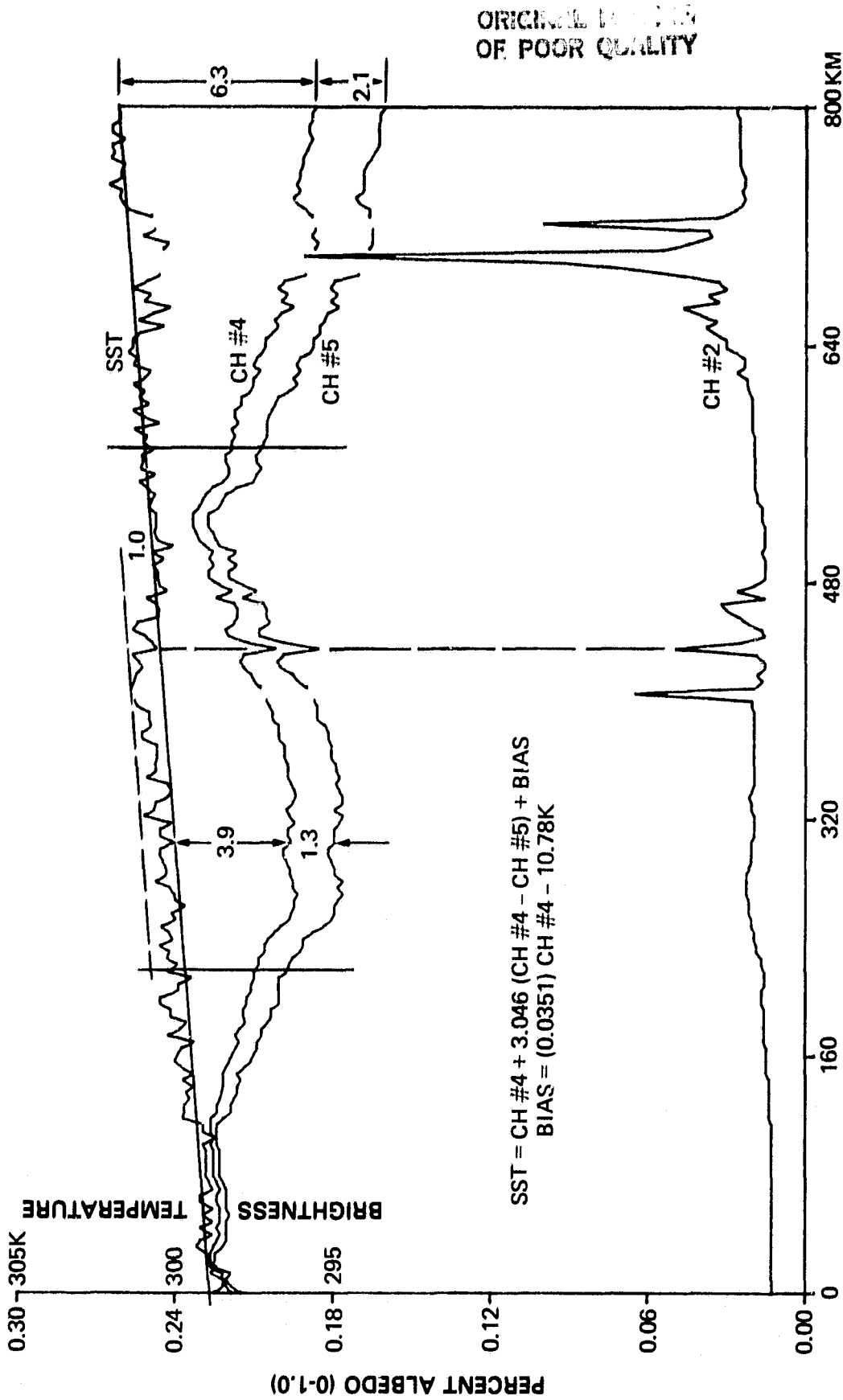
SST Example from NOAA-7 AVHRR, October 1981, Day 276

FIGURE 5
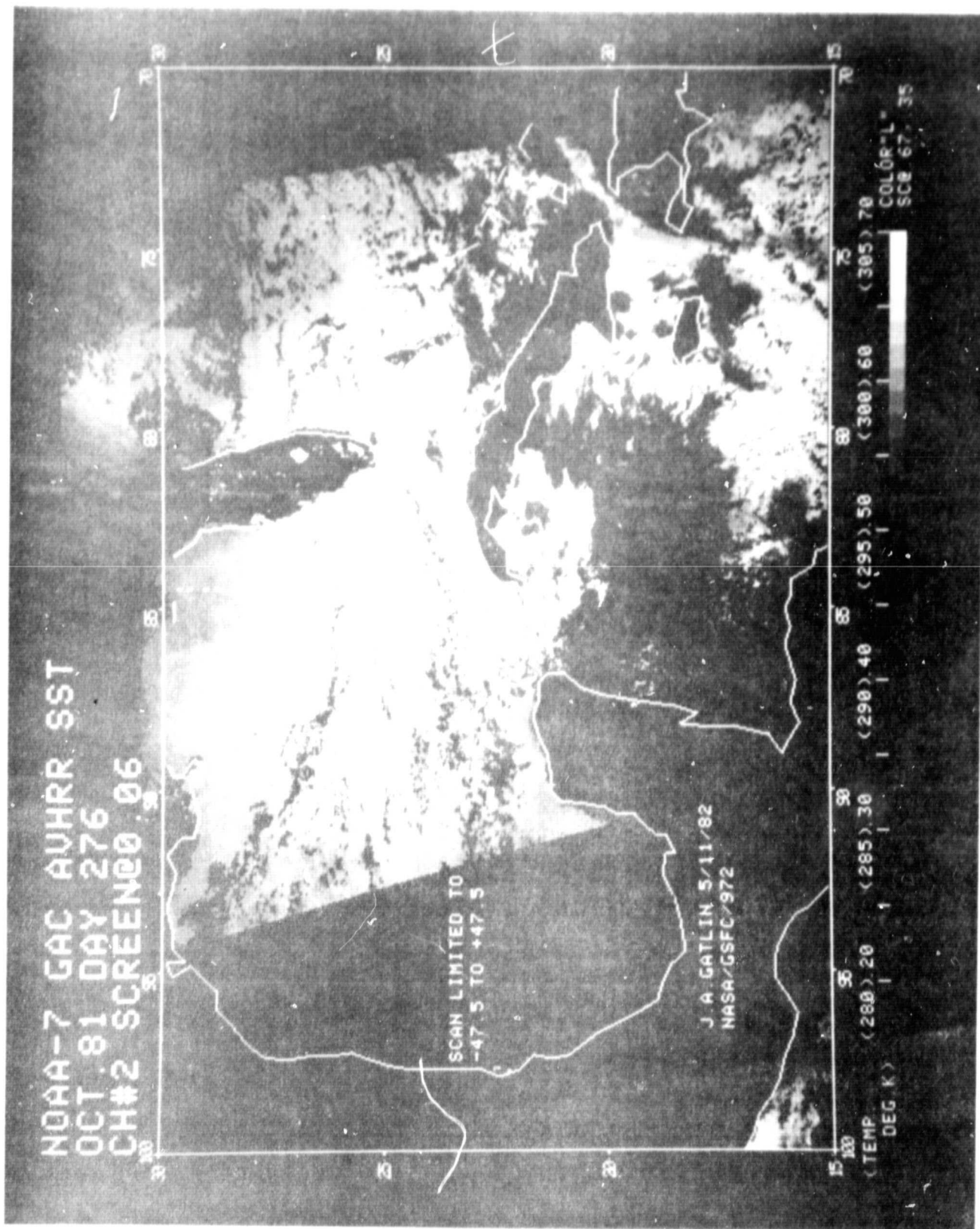
SST IMAGE DERIVED FROM THE SPLIT WINDOW ALGORITHM
FIGURE 6

WHOI/AVHRR
SINGLE POINT COMPARISON
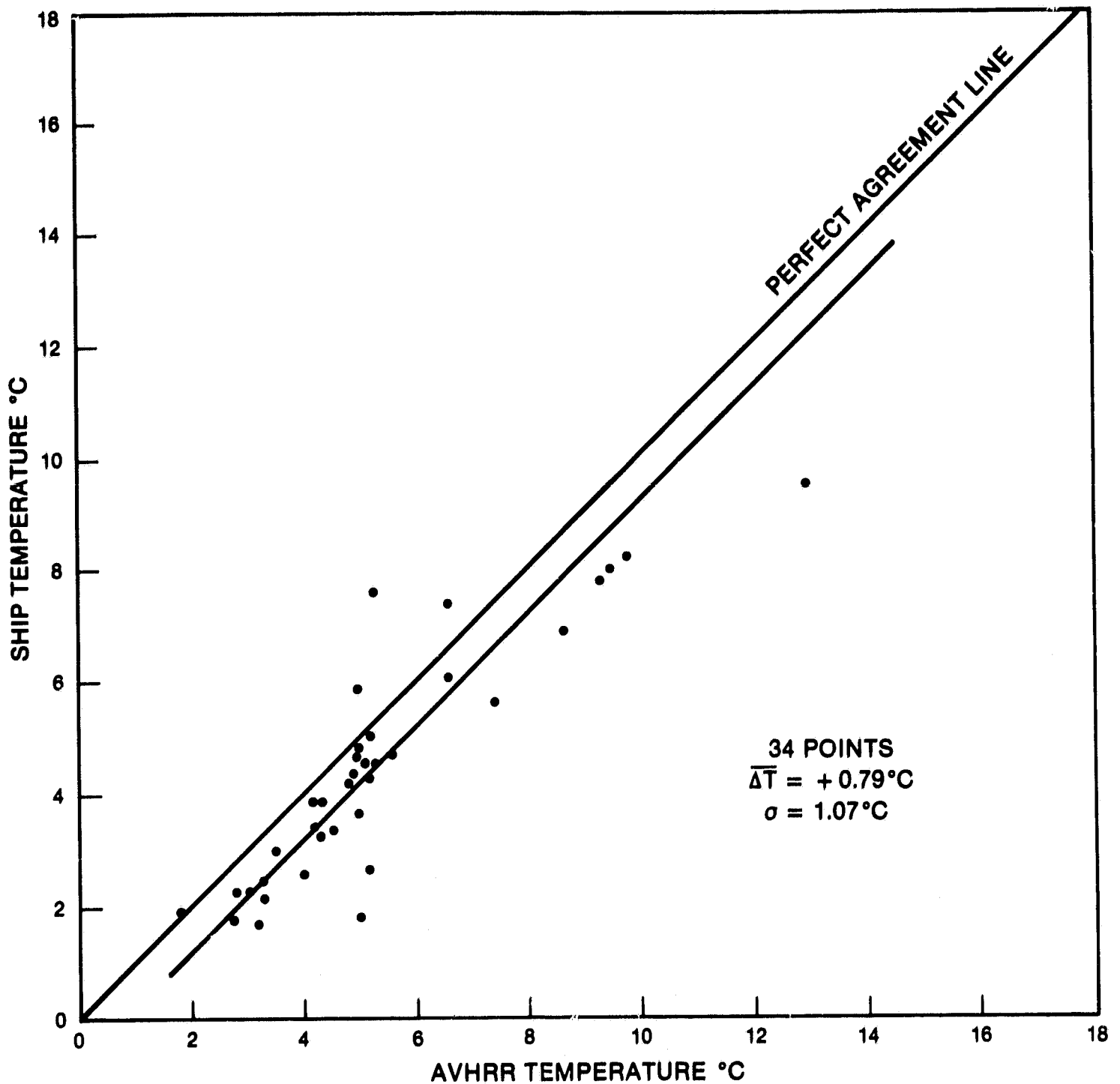
34 POINTS
$\overline{\Delta T} = +0.79°C$
$\sigma = 1.07°C$

FIGURE 7

WHOI/AVHRR
2km × 2km COMPARISON

PERFECT AGREEMENT LINE

35 POINTS
$\overline{\Delta T}$ = −0.28°C
σ = 0.96°C

AVHRR TEMPERATURE °C

SHIP TEMPERATURE °C

FIGURE 8

WHOI/AVHRR
10km × 10km COMPARISON

PERFECT AGREEMENT LINE

35 POINTS
$\overline{\Delta T}$ = + 0.62°C
σ = 1.30°C
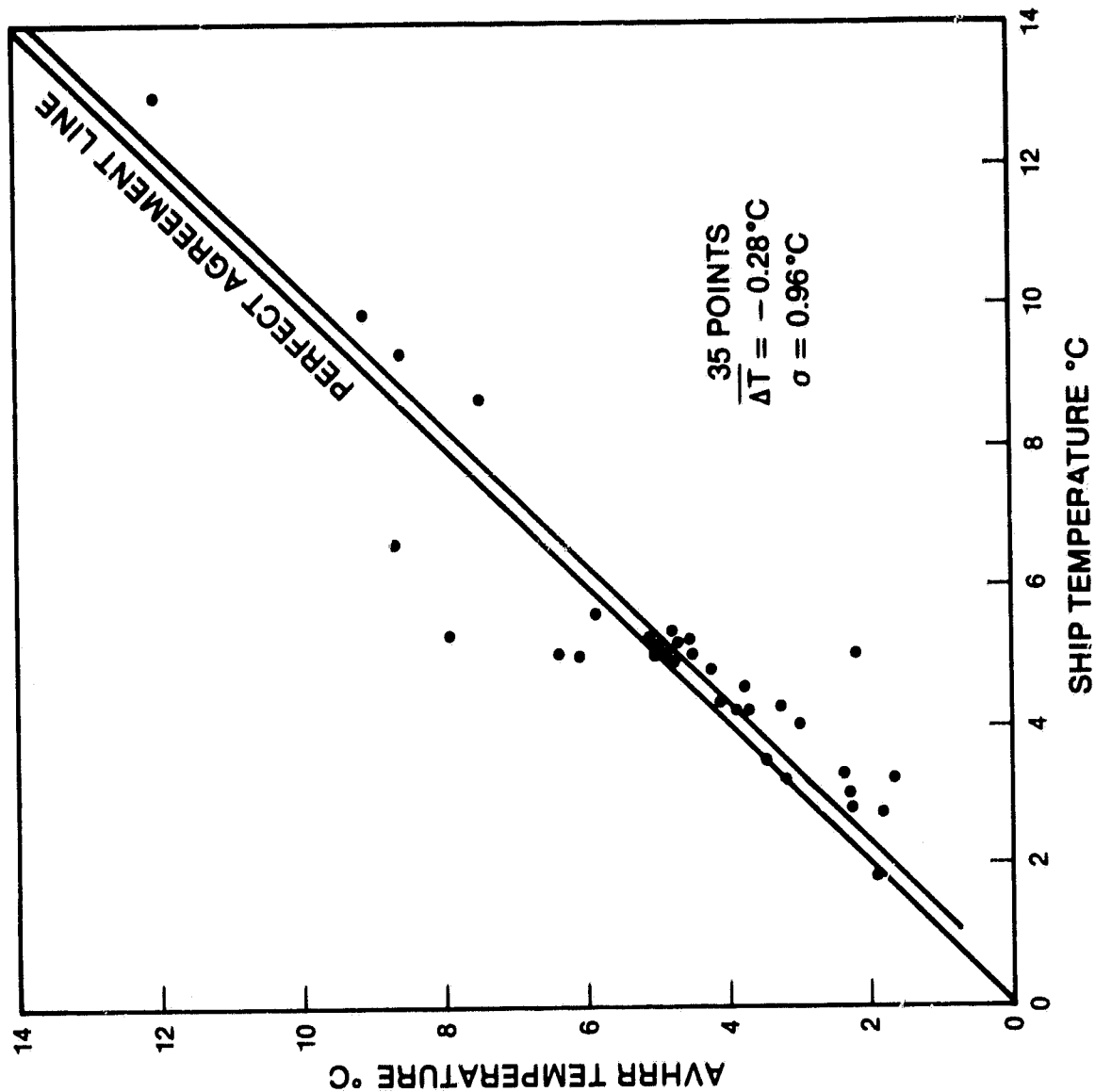
AVHRR TEMPERATURE °C
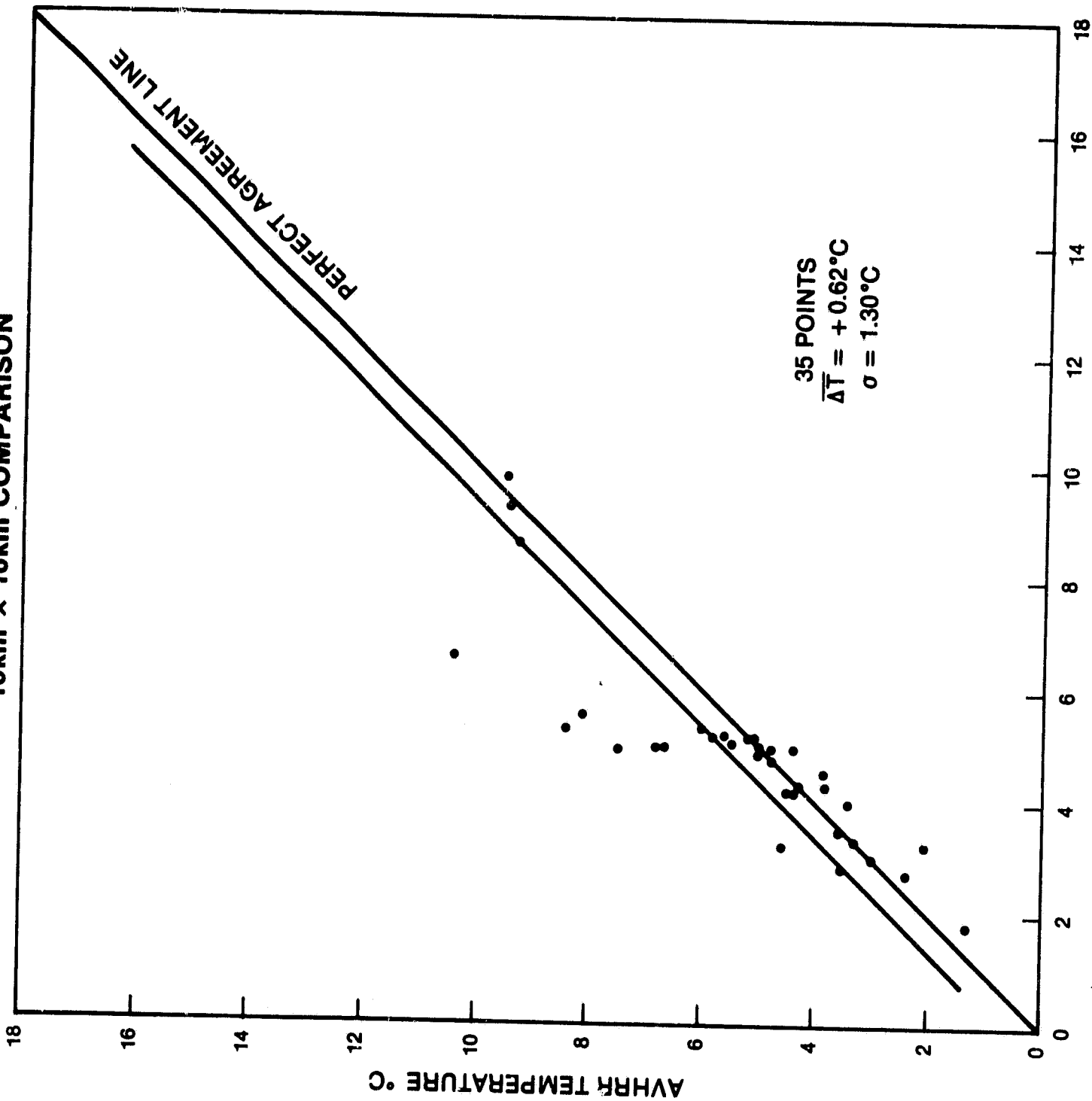
SHIP TEMPERATURE °C
FIGURE 9

WOODS HOLE CRUISE DATA 1/27/82
AVHRR TRACK ALONG 71.42°W.
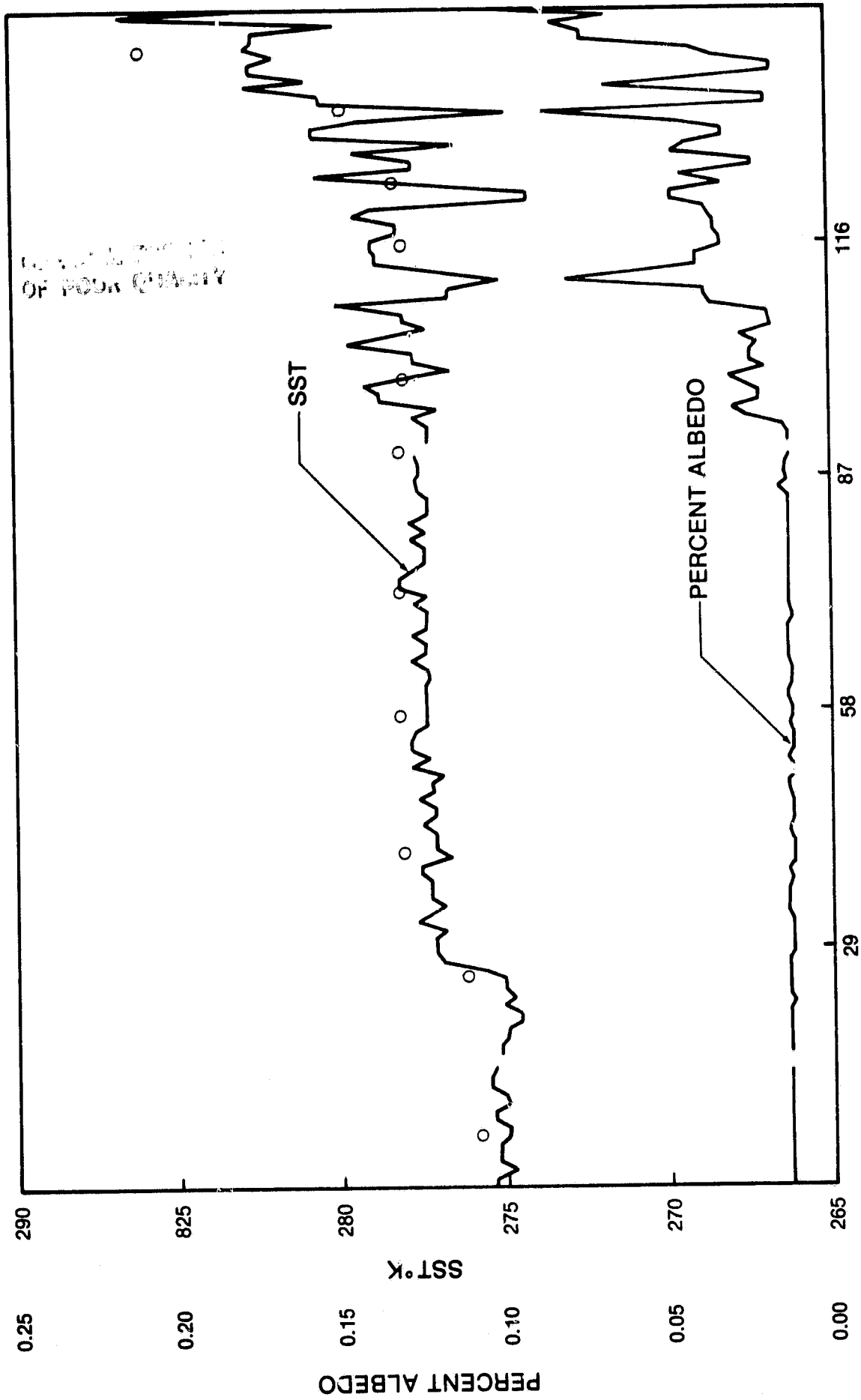
FIGURE 10

28

STUDY AREA

100m

40m

200m

400m

24

85

81
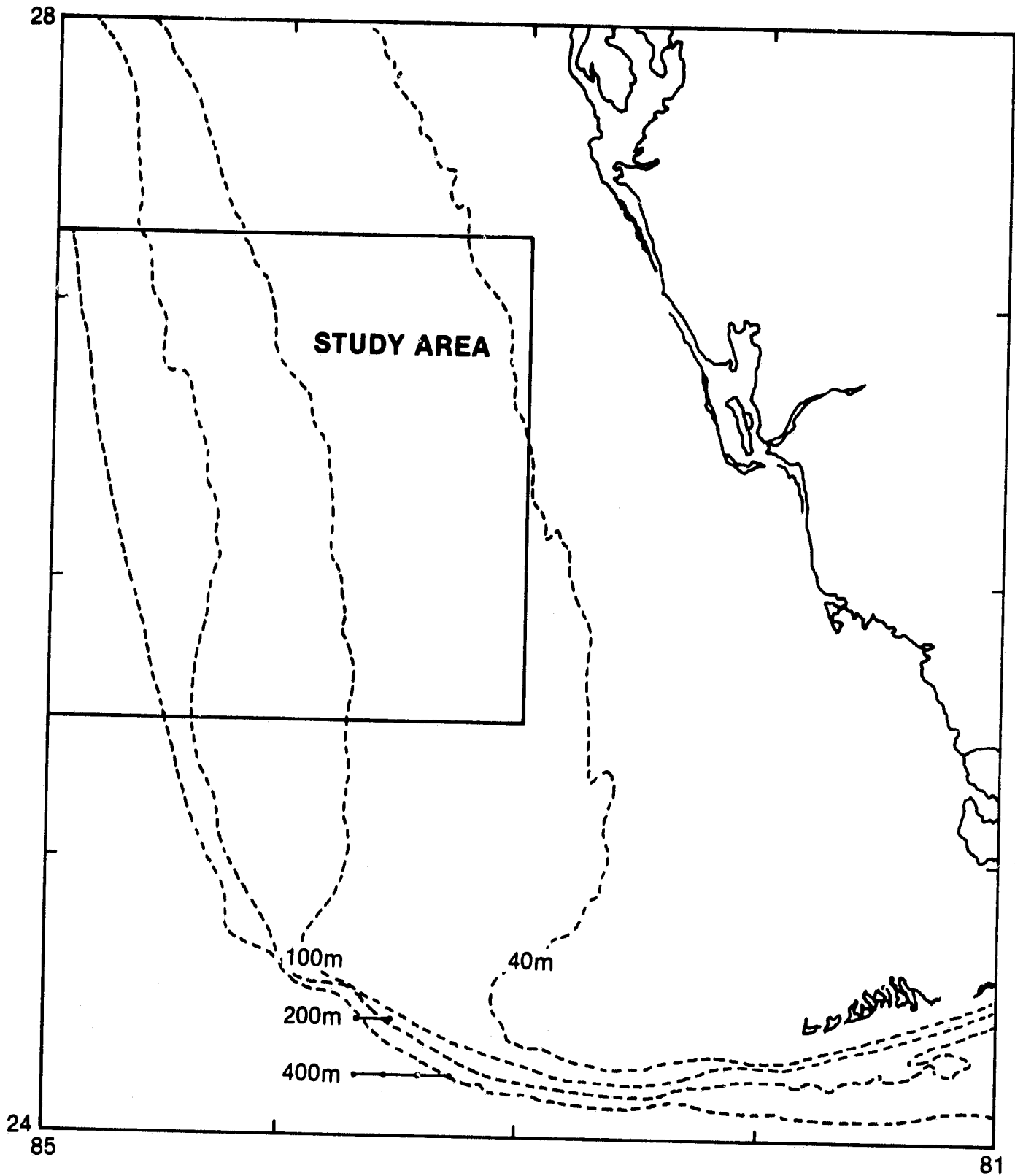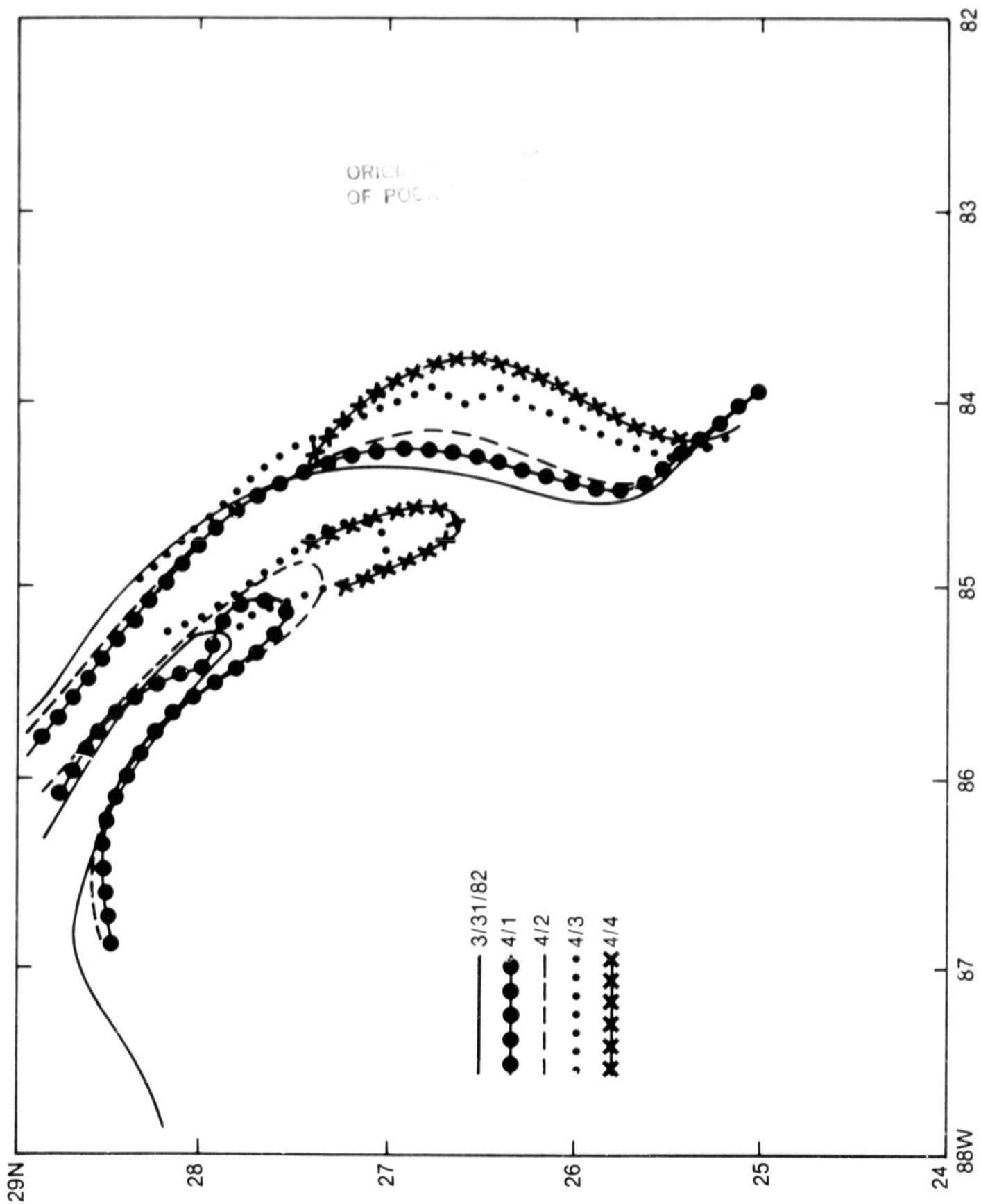
FIGURE 11

FIGURE 12

WEST FLORIDA SHELF
SPRING DATA SET
SINGLE POINT
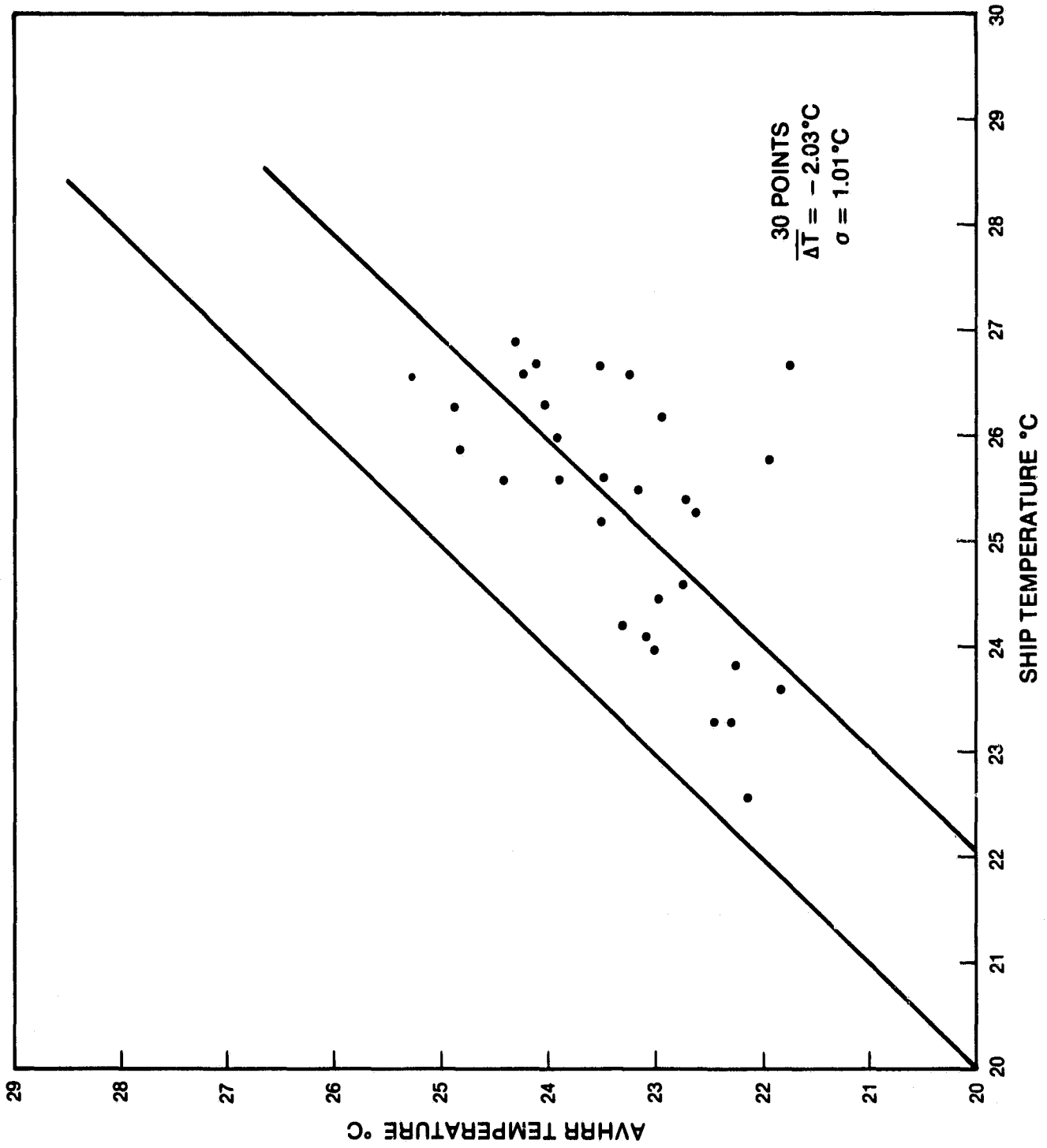
30 POINTS
$\overline{\Delta T}$ = −2.03°C
σ = 1.01°C

SHIP TEMPERATURE °C

AVHRR TEMPERATURE °C

FIGURE 13

WEST FLORIDA SHELF
SPRING DATA SET
2km × 2km AREA
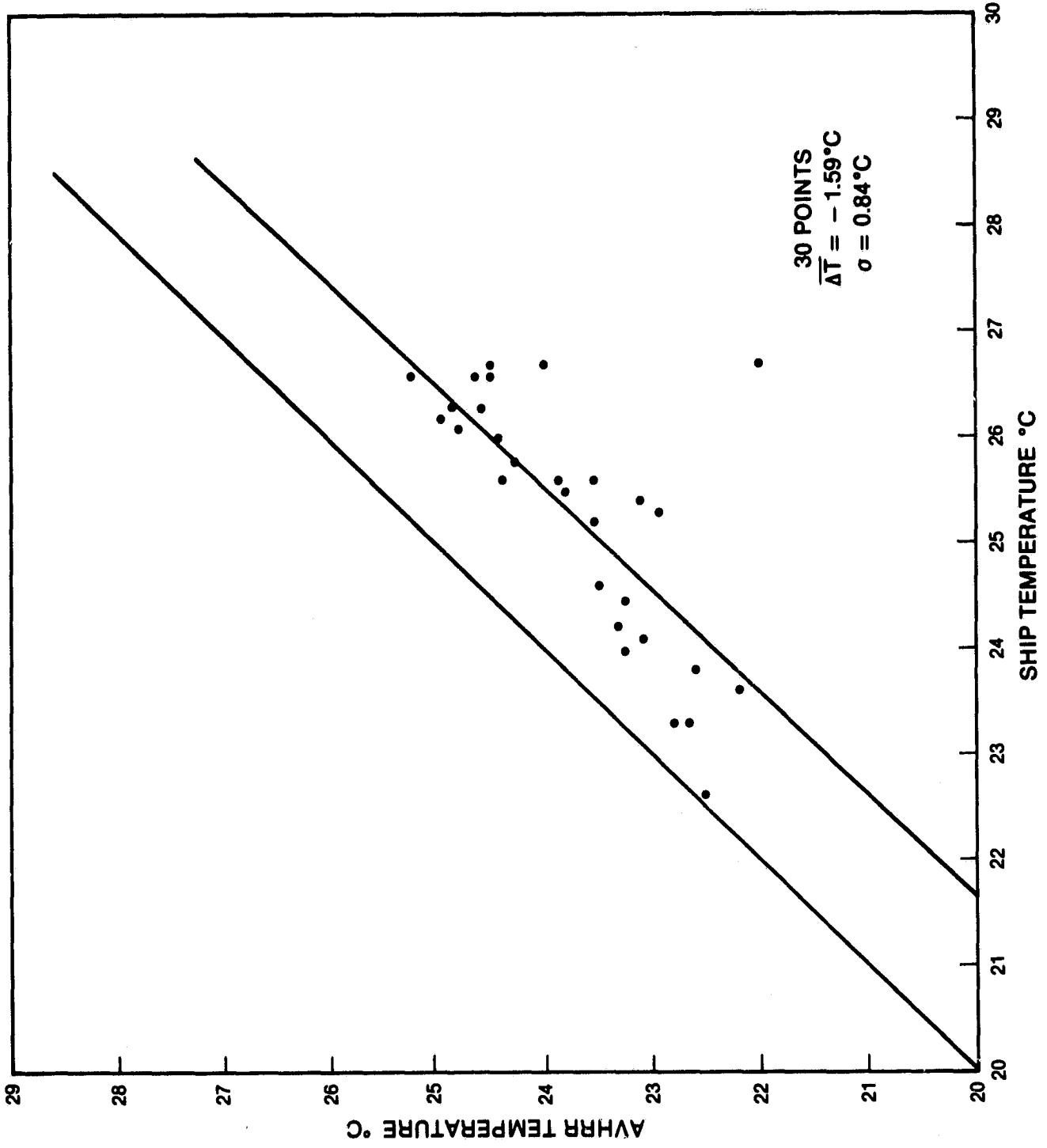
30 POINTS
$\overline{\Delta T} = -1.59°C$
$\sigma = 0.84°C$

AVHRR TEMPERATURE °C

SHIP TEMPERATURE °C

FIGURE 14

WEST FLORIDA SHELF
SPRING DATA SET
10km × 10km AREA

31 POINTS
$\overline{\Delta T}$ = −1.2°C
σ = 0.74°C

AVHRR TEMPERATURE °C

SHIP TEMPERATURE °C
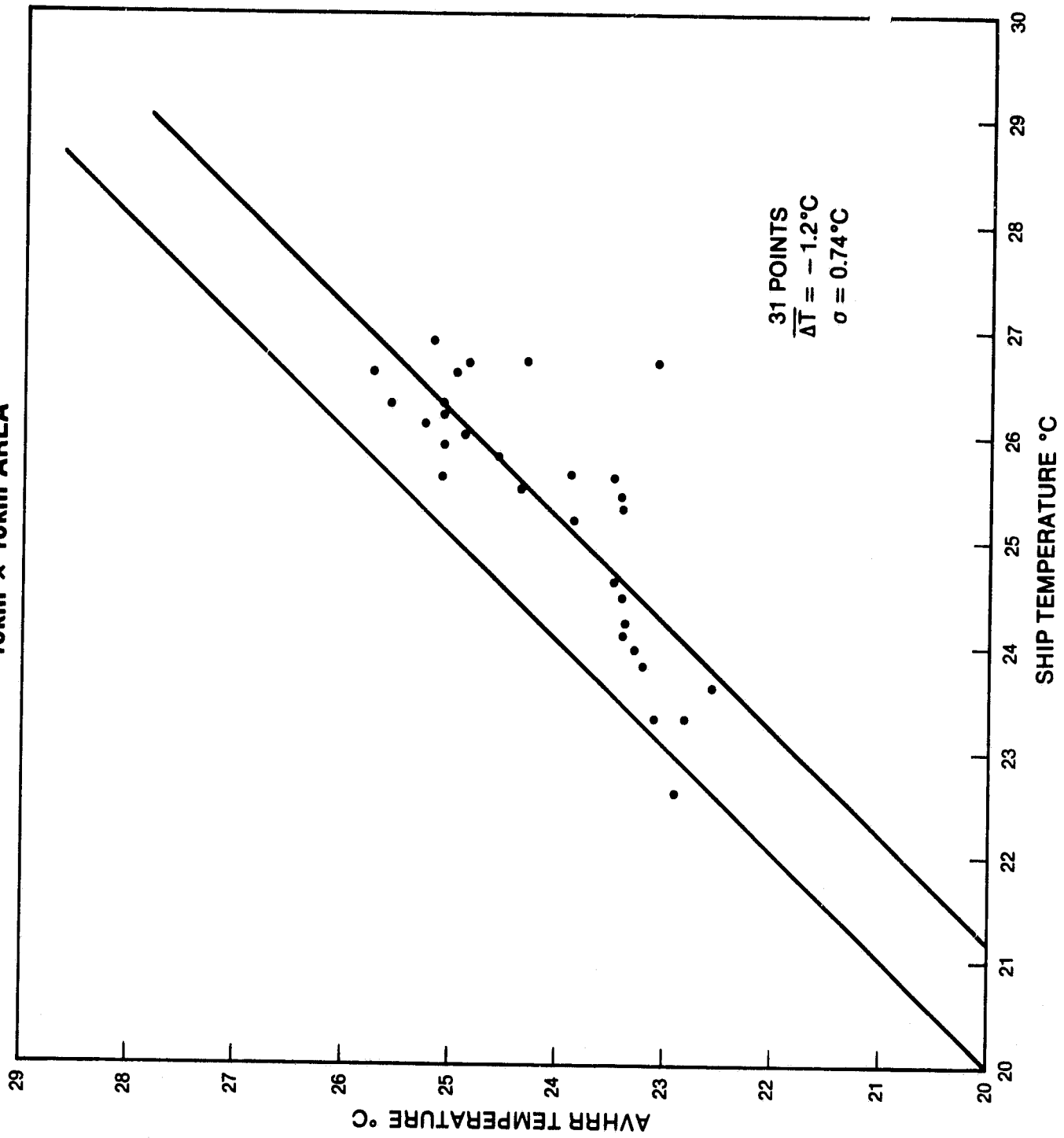
FIGURE 15

**WEST FLORIDA SHELF
FALL DATA SET
SINGLE POINT**
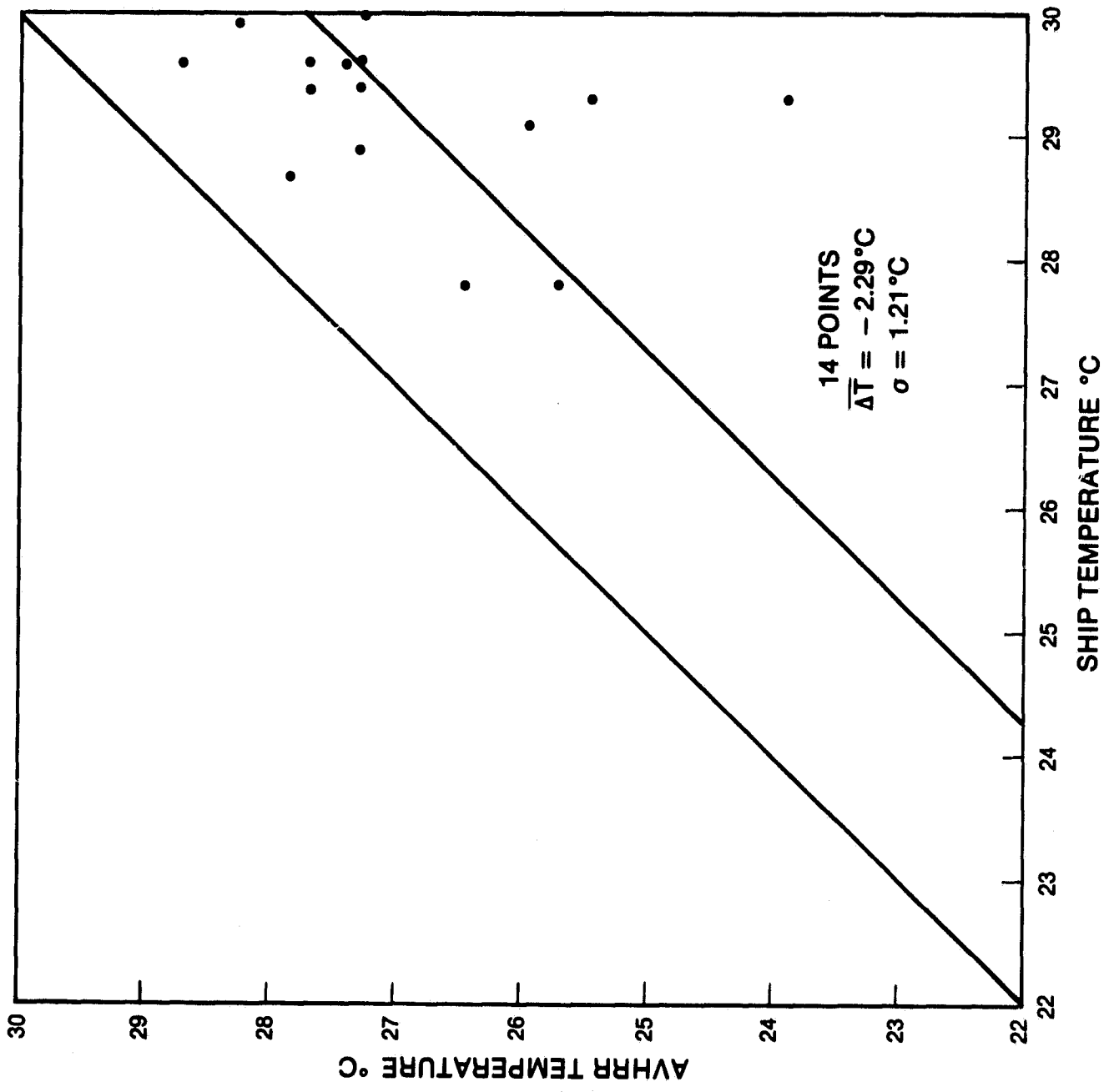
14 POINTS
$\overline{\Delta T} = -2.29°C$
$\sigma = 1.21°C$

SHIP TEMPERATURE °C

AVHRR TEMPERATURE °C

FIGURE 16

**WEST FLORIDA SHELF
FALL DATA SET
2km × 2km AREA**

14 POINTS
$\overline{\Delta T} = -1.68°C$
$\sigma = 0.61°C$

AVHRR TEMPERATURE °C

SHIP TEMPERATURE °C
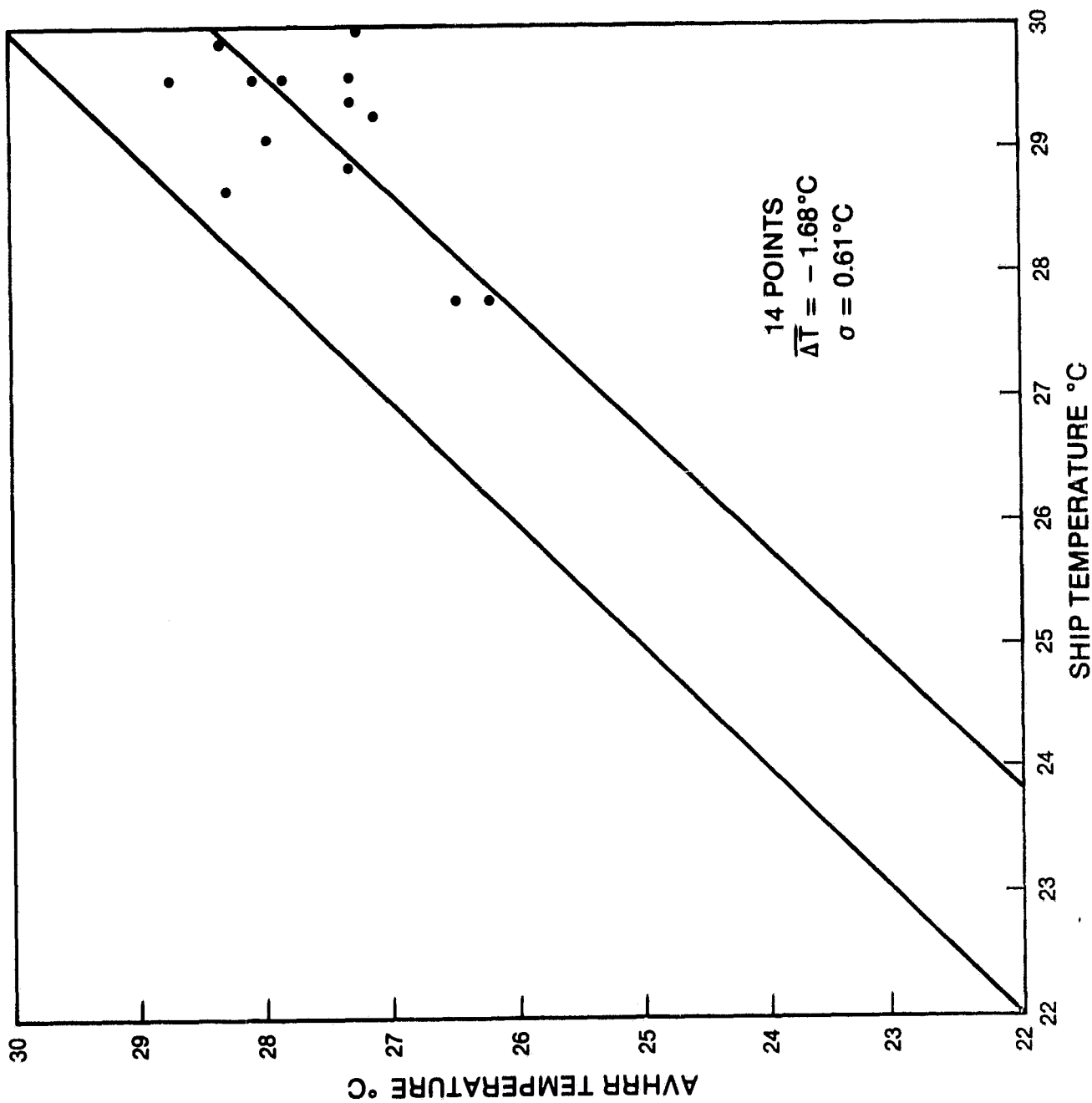
FIGURE 17

WEST FLORIDA SHELF
FALL DATA SET
10km x 10km AREA

16 POINTS
$\overline{\Delta T}$ = −1.17°C
σ = 0.73°C

AVHRR TEMPERATURE °C

SHIP TEMPERATURE °C

FIGURE 18

**18-22 APRIL 1982
SURFACE TEMP.**
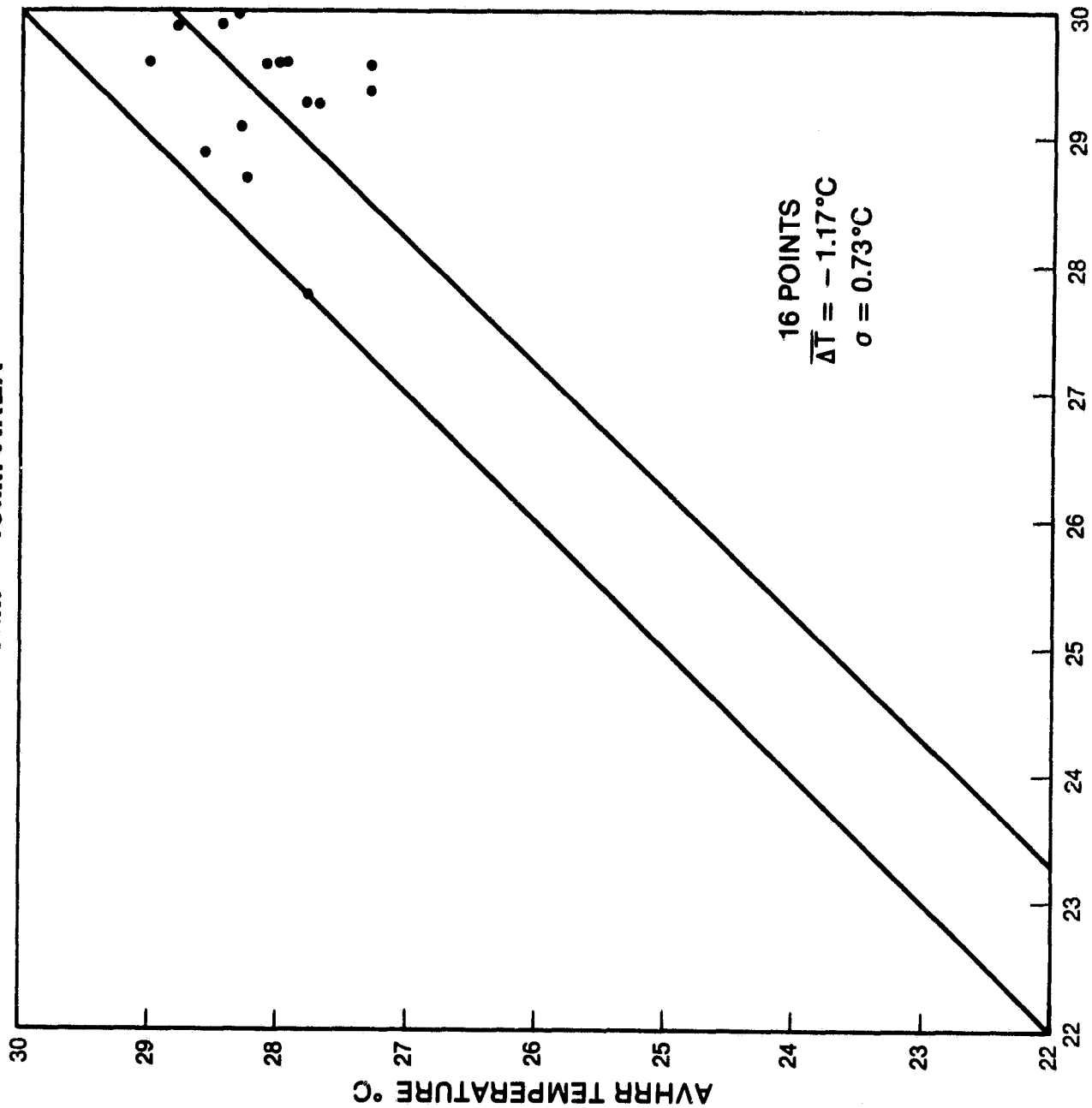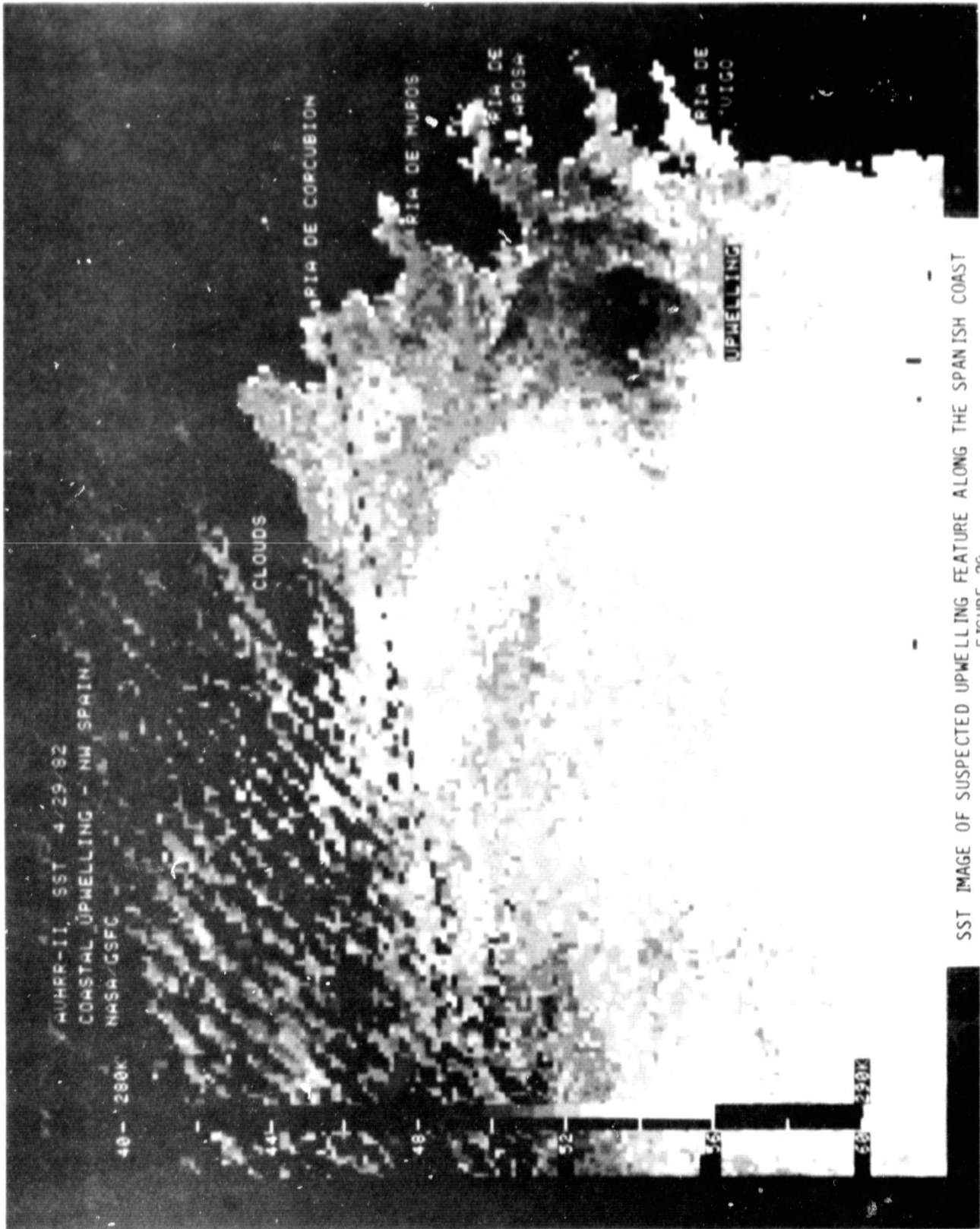
FIGURE 19

SST IMAGE OF SUSPECTED UPWELLING FEATURE ALONG THE SPANISH COAST
FIGURE 20

SPANISH COAST 4/29/82
MIDDLE OF THE FEATURE

FIGURE 21

SST

CH #5

CH #4
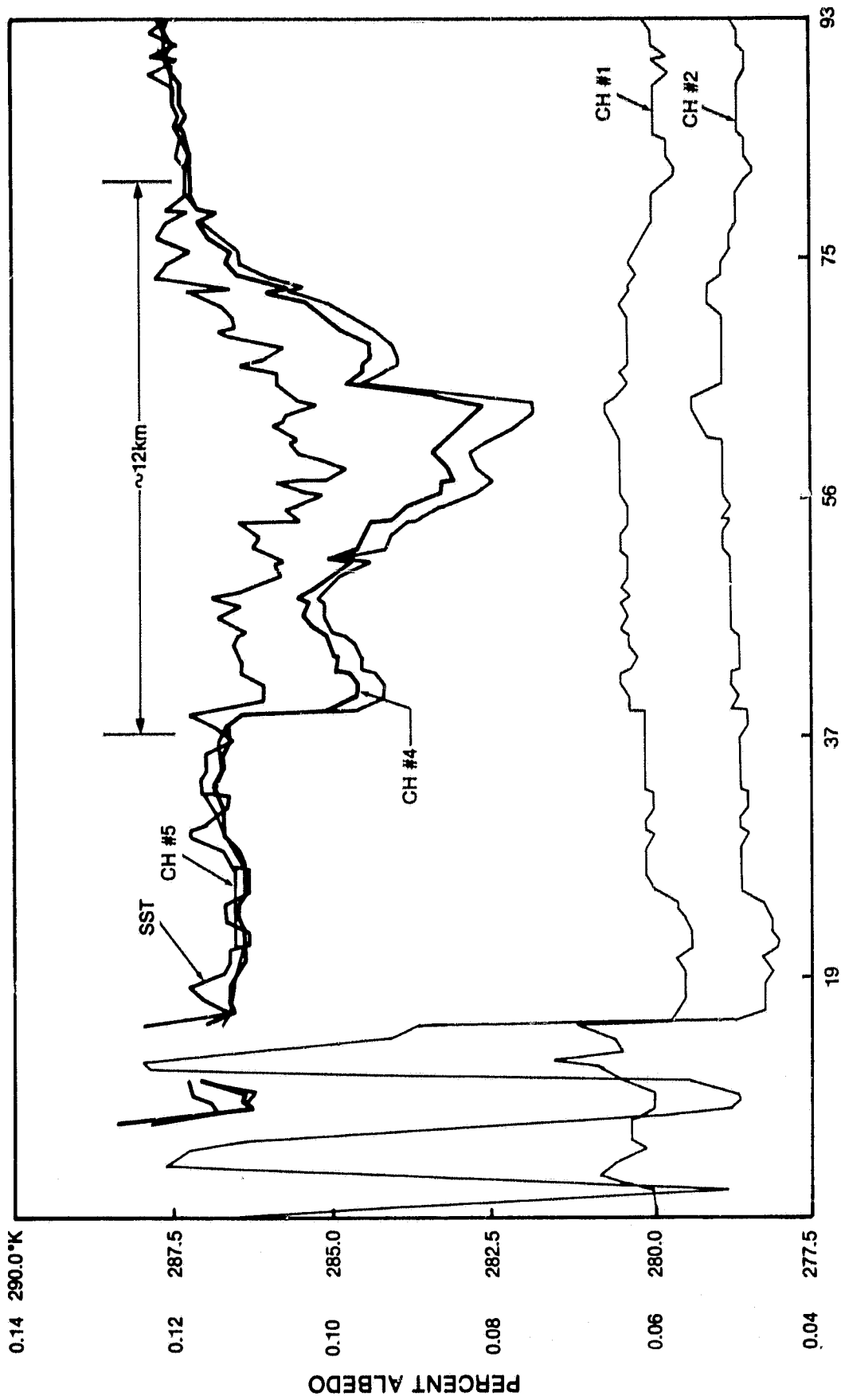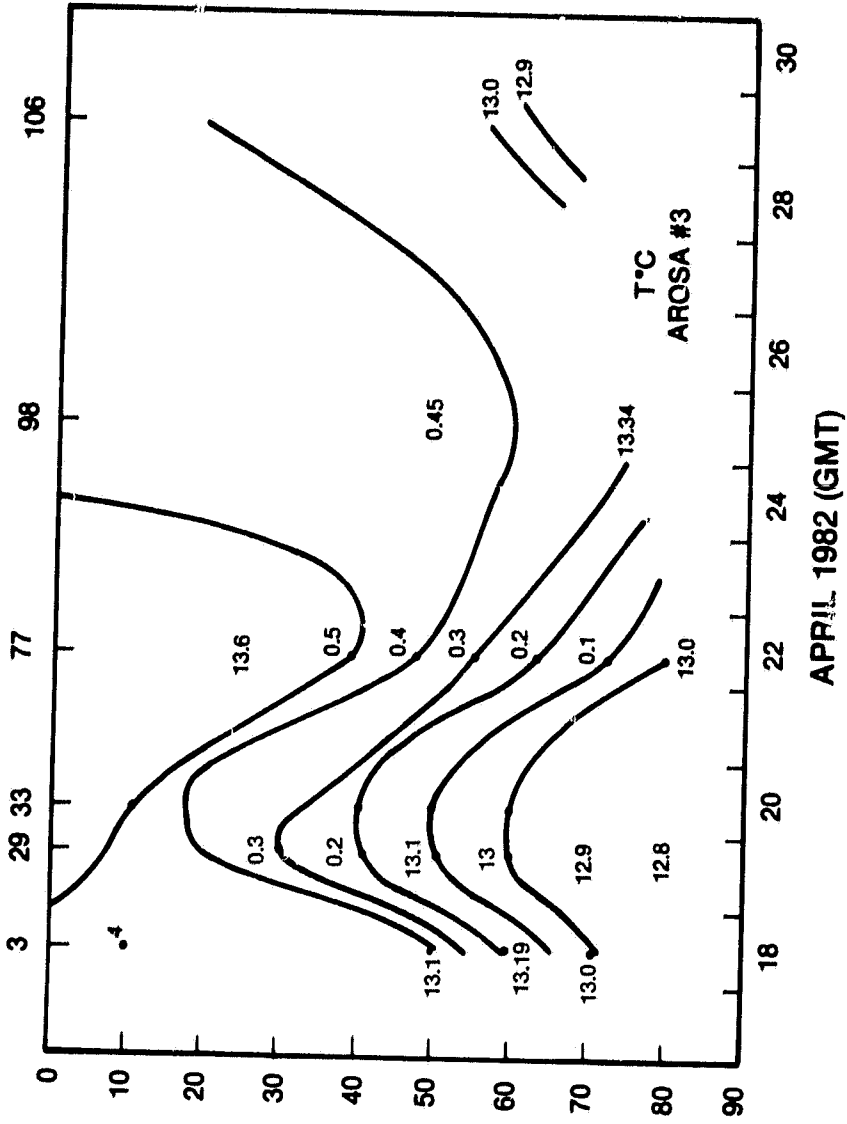
CH #1

CH #2

~12km

SOUTHERNMOST
POINT OF THE
TRACK

PERCENT ALBEDO

0.14   290.0°K

0.12   287.5

0.10   285.0

0.08   282.5

0.06   280.0

0.04   277.5

93

75

56

37

19

FIGURE 22. TIME SERIES OF TEMPERATURE AT STATION #3, RIA DE AROSA

FIGURE 22

WIND STRESS

N

0.1 NEWTON/m^2

APRIL 1982

FIGURE 23

UPWELLING INDEX

APRIL 1982

FIGURE 24